Multibody Syst Dyn (2010) 24: 133–166
DOI 10.1007/s11044-010-9213-z

Recursive formulations for multibody systems with frictional joints based on the interaction between bodies

Zhaohui Qi · Yongsheng Xu · Xiaoming Luo · Shengji Yao

Received: 2 September 2009 / Accepted: 20 May 2010 / Published online: 15 June 2010

Abstract In practice, the clearances of joints in a great number of mechanical systems are well under control. In these cases, some of the existing methods become unpractical because of the little differences in the order of magnitude between relative movements and computational errors. Assuming that the effects of impacts are negligible, we proved that both locations and forces of contacts in joints can be fully determined by parts of joint reaction forces. Based on this fact, a method particularly suited for multibody systems possessing frictional joints with tiny clearances is presented. In order to improve the efficiency of computation, recursive formulations are proposed based on the interactions between bodies. The proposed recursive formulations can improve the computation of joint reaction forces. With the methodology presented in this paper, not only the motion of bodies in a multibody system but also the details about the contacts in joints, such as forces of contacts and locations of contact points, can be obtained. Even with the assumption of impact free, the instants of possible impacts can be detected without relying upon any ambiguous parameters, as indicated by numerical examples in this paper.

Keywords Multibody systems · Frictional joints · Recursive formulation

1 Introduction

With significant applications in engineering, multibody system dynamics has become an important computational tool, which in turn generates a demand for more accurate analysis of real mechanical systems. Traditionally, dynamic analysis of multibody systems was conducted by assuming that the joints were perfect, that means the effects of collision and friction in the joints were neglected. Friction is one of the most common physical phenomena in

Z. Qi (✉) · Y. Xu · X. Luo
State Key Laboratory of Structural Analysis for Industrial Equipment, Dalian University of Technology, 116024, Dalian, China
e-mail: zhaohuiq@dlut.edu.cn

S. Yao
Department of Mechanical Engineering, University of New Brunswick, NB, E3B 5A3, Fredericton, Canada

everyday life. It is possible to reduce the friction, but impossible to eliminate it completely. Sometimes it can significantly affect the dynamic response of multibody systems.

Over the past decades, a great deal of research on contact dynamics have been carried out [1, 2]. The majority of them focused on the general subject such as multiple contacts with collision between bodies with arbitrary shape. According to the literature, contact modeling consists of two major parts: evaluating contact forces and detecting locations of contact points.

In general, there are two different approaches for modeling contact forces. The first approach, referred to as a discrete method, assumes that there is no penetration between the contacting bodies and the collision occurs instantaneously [3–7]. As additional variables, contact forces are introduced into the equations of motion and solved by unilateral contact conditions and impact laws. However, because too much physical information about the impact is lost, different impact laws do not always produce the same results [8–12], especially when Coulomb friction is considered. The Coulomb's law leads to a linear or nonlinear complementary formulation of the system model depending on the plane or spatial character of the contacts [13, 14]. The equations of motion during an impact free phase are quite different from those during an impact phase. In order to deal with this switching nature, event-driven and time-stepping numerical schemes are proposed [15, 16].

The second approach, referred to as a continuous method, assumes that two contacting bodies can penetrate each other whereas the normal contact forces vary continuously with respect to the penetration and the corresponding rate. With this model, the formulation of frictional forces can be greatly simplified because the contact forces become an explicit function of system state variables [17–21]. But the continuous method has two major drawbacks. One is that the parameters in the force model are not certain and the other one is that the steps of numerical integration must be very small in order to accurately evaluate the penetration depths.

One of the most critical aspects in the contact dynamics is to detect precisely the instant and locations of contacts. In spite of obvious differences in contact force models, algorithms for contact detection have little differences in principle. In most of the relevant methods, a group of gap functions are employed for the computation of distances between potential contact points, and the values of the gap functions must be kept under control [2, 22–27]. When multiple contacts take place frequently, the contact detection can be very time-consuming.

In practice, there is an important class of joints, such as well-made joints, in which the clearances are so tiny that the effect of collision is negligible. In this case, an explicit closed-form solution for the normal contact forces at the contact points can be obtained by the method proposed in [28]. However, instead of becoming a little bit easier, the contact detection becomes unpractical with the aforementioned method because computational errors and the range of the relative motion between the two bodies linked by such kind of joint are usually in the same order of magnitude. Paul [29] and Hall [30] described an alternative methodology for contact detection in their textbooks, based on the relation between the joint reaction forces and the contact forces in the joint. This relation is dependent on the contact models. According to Paul and Hall, all possible contact models should be established in advance and the real contact model is identified iteratively according to which model is consistent with the joint reaction forces. Their applications in planar mechanism were investigated by Haug et al. [31]. The main advantage of this approach is that it does not require the calculation of the relative motion in joints. However, except for simple contact scenarios, it is difficult to manually enumerate all possible contact models.

It seems that there is a trade-off between the efficiency of computations and the details in contacts. Placing emphasis on the computational efficiency, the general purpose software

ADAMS provides a force model for each classic type of joints, from which the frictional forces in joints can be calculated by joint reaction forces, but the corresponding forces and locations of contacts cannot be deduced.

Based on the fact that the locations and forces of contacts in a joint can fully determine the joint reaction forces and vice versa, which will be shown in this paper, we present a methodology for the analysis of multibody systems with non-colliding but frictional contacts in the joints, with which both contact forces and contact locations can be obtained in a programmable way.

The paper is arranged as follows. In Sect. 2, kinematical recursive relations between two constrained bodies are reviewed. In Sect. 3, we present a method of recursively reducing a multibody system with the tree structure to an equivalent system with one of the tree-end bodies removed. This method serves as a basis of formulating complex multibody systems. Different from the existing recursive methods [32–36] that primarily focus on the mathematic procedure, the recursive method proposed in this paper attaches much importance on the physical insight. In Sect. 4, a systematic way to generate constraint equations of cut joints is described. Section 5 deals with the description of joint reaction forces of frictional joints. In Sect. 6, recursive formulations of general multibody systems are given by taking the frictional forces and joint reaction forces of cut joints as external applied forces. In Sect. 7, equations to determine the frictional forces are presented for some typical joints. Finally, Sect. 8 gives some numerical examples to demonstrate the application of the methodology presented in this paper. Section 9 concludes this paper.

2 Kinematical recursive relations

In this section, we will briefly review the kinematical recursive relations between a pair of bodies in a multibody system with an open tree topology. We assume that the number of bodies and joints are regularly labeled [38], or more exactly, body i is connected to its inboard body $\underline{i}$ by joint i, where the inboard body of body i is referred to the lower adjacent connecting body to body i and its label is denoted by $\underline{i}$ in this paper, as shown in Fig. 1, where $p_{\underline{i}}$ and p_i are the joint definition points on body $\underline{i}$ and body I, respectively; meanwhile $\mathbf{r}_{\underline{i}}$ and $\mathbf{r}_i$ are the position vectors of the origins of the reference frame attached to body $\underline{i}$ and body I, respectively.

If joint i allows translational degrees of freedom, the vector between $p_{\underline{i}}$ and p_i can be expressed in matrix form

$$\mathbf{s}_i = \mathbf{P}_i^s \mathbf{q}_i, \tag{1}$$

where $\mathbf{q}_i$ is the vector of the joint coordinates and $\mathbf{P}_i^s$ is the matrix whose nonzero columns are composed of the joint translational axis vectors. If the joint allows rotational degrees of freedom, the joint angular velocity can be expressed in matrix form

$$\bar{\boldsymbol{\omega}}_i = \mathbf{P}_i^r \dot{\mathbf{q}}_i \tag{2}$$

in which $\mathbf{P}_i^r$ is the matrix whose non-zero columns are composed of the joint rotational axis vectors [32]. Consequently, $\boldsymbol{\omega}_i$, the angular velocity of body i and $\boldsymbol{\omega}_{\underline{i}}$, the angular velocity of body $\underline{i}$ are related to each other by the following equation:

$$\boldsymbol{\omega}_i = \boldsymbol{\omega}_{\underline{i}} + \mathbf{P}_i^r \dot{\mathbf{q}}_i. \tag{3}$$

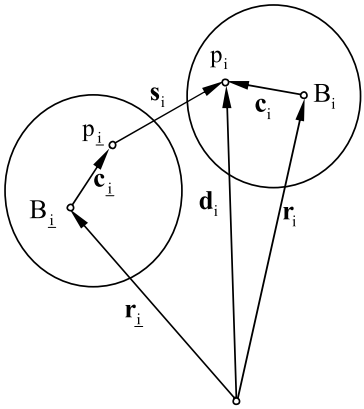

Fig. 1 A pair of contiguous bodies

As indicated in Fig. 1, the absolute position vector of the origin of reference frame of body i is

$$\mathbf{r}_i = \mathbf{r}_{\underline{i}} + c_{\underline{i}} + s_i - c_i, \tag{4}$$

where $\mathbf{c}_{\underline{i}}$ is the vector from the origin point of body reference frame of body $\underline{i}$ to the joint definition point $p_{\underline{i}}$, and $\mathbf{c}_i$ is defined exactly in the same manner. When the joint provides both translational and rotational degrees of freedom, the rotational center of the joint around which the two connected bodies rotate with respect to each other should be defined. Conventionally, the rotational center is located at either point $p_{\underline{i}}$ or point p_i, and its position vector is given by $\mathbf{d}_i = \mathbf{r}_{\underline{i}} + \mathbf{c}_{\underline{i}}$ or $\mathbf{d}_i = \mathbf{r}_i + \mathbf{c}_i$ accordingly.

The time derivative of (4) shows the recursive relations between the translational velocities of body i and body $\underline{i}$. It can be expressed as

$$\dot{\mathbf{r}}_i = \dot{\mathbf{r}}_{\underline{i}} + (\tilde{\mathbf{r}}_{\underline{i}} - \tilde{\mathbf{r}}_i)\boldsymbol{\omega}_{\underline{i}} + \left(\mathbf{P}_i^s + (\tilde{\mathbf{d}}_i - \tilde{\mathbf{r}}_i)\mathbf{P}_i^r\right)\dot{\mathbf{q}}_i, \tag{5}$$

where the tilde operator is defined as follows: it acts on a vector $\mathbf{a}$ to produce the skew-symmetric matrix $\tilde{\mathbf{a}}$ such that $\mathbf{a} \times \mathbf{b} = \tilde{\mathbf{a}}\mathbf{b}$. Equations (3) and (5) can be written together in compact form as

$$\mathbf{Z}_i = \boldsymbol{\Gamma}_i \mathbf{Z}_{\underline{i}} + \boldsymbol{\Pi}_i \dot{\mathbf{q}}_i, \tag{6}$$

where

$$\mathbf{Z}_i = \begin{bmatrix} \dot{\mathbf{r}}_i \\ \boldsymbol{\omega}_i \end{bmatrix}, \quad \mathbf{Z}_{\underline{i}} = \begin{bmatrix} \dot{\mathbf{r}}_{\underline{i}} \\ \boldsymbol{\omega}_{\underline{i}} \end{bmatrix}, \quad \boldsymbol{\Gamma}_i = \begin{bmatrix} \mathbf{I} & \tilde{\mathbf{r}}_{\underline{i}} - \tilde{\mathbf{r}}_i \\ \mathbf{0} & \mathbf{I} \end{bmatrix}, \quad \boldsymbol{\Pi}_i = \begin{bmatrix} \mathbf{P}_i^s + (\tilde{\mathbf{d}}_i - \tilde{\mathbf{r}}_i)\mathbf{P}_i^r \\ \mathbf{P}_i^r \end{bmatrix}. \tag{7}$$

According to (6), the relationship between the virtual velocities of two consecutive bodes is given as

$$\delta\mathbf{Z}_i = \boldsymbol{\Gamma}_i \delta\mathbf{Z}_{\underline{i}} + \boldsymbol{\Pi}_i \delta\dot{\mathbf{q}}_i. \tag{8}$$

Differentiating (3) with respect to time yields

$$\dot{\boldsymbol{\omega}}_i = \dot{\boldsymbol{\omega}}_{\underline{i}} + \mathbf{P}_i^r \ddot{\mathbf{q}}_i + \boldsymbol{\sigma}_i, \tag{9}$$

where $\boldsymbol{\sigma}_i$ is the angular velocity of body i when $\dot{\boldsymbol{\omega}}_{\underline{i}}$ and $\ddot{\mathbf{q}}_i$ are zero vectors. For examples,

$$\boldsymbol{\sigma}_i = \boldsymbol{\omega}_{\underline{i}} \times \bar{\boldsymbol{\omega}}_i + \begin{cases} \mathbf{0} & \\ \quad \text{for revolute, cylindrical and prismatic joints,} & \\ \mathbf{p}^r_{i1} \times \mathbf{p}^r_{i2} \dot{q}_{i1} \dot{q}_{i2} & \text{for universal joints,} \\ \mathbf{p}^r_{i1} \times \mathbf{p}^r_{i2} \dot{q}_{i1} \dot{q}_{i2} + \dot{q}_{i3} \dot{q}_{i1} \mathbf{p}^r_{i1} \times \mathbf{p}^r_{i3} + \dot{q}_{i2} \dot{q}_{i3} \mathbf{p}^r_{i2} \times \mathbf{p}^r_{i3} & \text{for spherical joints,} \end{cases} \tag{10}$$

where $\mathbf{p}^r_{ik}$ is the vector of the kth rotational axis of joint i and $\dot{q}_{ik}$ is the time derivative of the kth joint coordinate of joint i. The translational acceleration of body i can be expressed as

$$\ddot{\mathbf{r}}_i = \ddot{\mathbf{r}}_{\underline{i}} + (\tilde{\mathbf{r}}_{\underline{i}} - \tilde{\mathbf{r}}_i)\dot{\boldsymbol{\omega}}_{\underline{i}} + \mathbf{P}^s_i \ddot{\mathbf{q}}_i + (\tilde{\mathbf{d}}_i - \tilde{\mathbf{r}}_i)\mathbf{P}^r_i \ddot{\mathbf{q}}_i + \boldsymbol{\gamma}_i, \tag{11}$$

where $\boldsymbol{\gamma}_i$ is the translational acceleration of body i when $\dot{\boldsymbol{\omega}}_{\underline{i}}$, $\ddot{\mathbf{r}}_{\underline{i}}$, and $\ddot{\mathbf{q}}_i$ all vanish. If point p_i is the rotational center of joint i, then

$$\boldsymbol{\gamma}_i = \tilde{\boldsymbol{\omega}}_{\underline{i}} \tilde{\boldsymbol{\omega}}_{\underline{i}} (\mathbf{d}_i - \mathbf{r}_{\underline{i}}) - (\tilde{\boldsymbol{\sigma}}_i + \tilde{\boldsymbol{\omega}}_i \tilde{\boldsymbol{\omega}}_i)(\mathbf{d}_i - \mathbf{r}_i) + 2\tilde{\boldsymbol{\omega}}_{\underline{i}} \mathbf{P}^s_i \dot{\mathbf{q}}_i. \tag{12}$$

If point $p_{\underline{i}}$ is the rotational center of joint i, then

$$\boldsymbol{\gamma}_i = \tilde{\boldsymbol{\omega}}_{\underline{i}} \tilde{\boldsymbol{\omega}}_{\underline{i}} (\mathbf{d}_i - \mathbf{r}_{\underline{i}}) - (\tilde{\boldsymbol{\sigma}}_i + \tilde{\boldsymbol{\omega}}_i \tilde{\boldsymbol{\omega}}_i)(\mathbf{d}_i - \mathbf{r}_i) + 2\tilde{\boldsymbol{\omega}}_i \mathbf{P}^s_i \dot{\mathbf{q}}_i. \tag{13}$$

Equations (9) and (11) can be written in a compact form as

$$\dot{\mathbf{Z}}_i = \boldsymbol{\Gamma}_i \dot{\mathbf{Z}}_{\underline{i}} + \boldsymbol{\Pi}_i \ddot{\mathbf{q}}_i + \mathbf{w}_i, \tag{14}$$

where $\mathbf{w}_i = [\boldsymbol{\gamma}_i \ \boldsymbol{\sigma}_i]^T$. The recursive kinematic relations represented by (6) and (14) are the basis of almost all the recursive formulations of multibody systems [31–37].

3 Dynamic decoupling of multibody systems with tree topology

In a multibody system with tree topology, the equations of motion of a single body i can be written as

$$\mathbf{M}_i \dot{\mathbf{Z}}_i - \mathbf{F}^0_i - \mathbf{F}^a_i - \mathbf{F}^c_i = \mathbf{0} \tag{15}$$

in terms of its matrix of mass $\mathbf{M}_i$, velocity dependent force $\mathbf{F}^0_i$, applied force $\mathbf{F}^a_i$ composed of resultant force and torque acting on the body i, and joint reaction force $\mathbf{F}^c_i$ exerted by all the joints attached to the body i, where

$$\mathbf{M}_i = \begin{bmatrix} m_i \mathbf{E} & -m_i \tilde{\mathbf{r}}_{ci} \\ m_i \tilde{\mathbf{r}}_{ci} & \mathbf{J}_i \end{bmatrix} \tag{16}$$

and

$$\mathbf{F}^0_i = -\begin{bmatrix} m_i \tilde{\boldsymbol{\omega}}_i \tilde{\boldsymbol{\omega}}_i \mathbf{r}_{ci} \\ \tilde{\boldsymbol{\omega}}_i \mathbf{J}_i \boldsymbol{\omega}_i \end{bmatrix}. \tag{17}$$

In these equations, $\mathbf{r}_{ci}$ is the vector from the origin of the reference frame to the mass center of body i, and $\mathbf{J}_i$ is its rotational inertia with respective to the origin of the reference frame. In accordance with (15), the joint reaction force $\mathbf{F}^c_n$ on the tree-end body n yields

$$\mathbf{F}^c_n = \mathbf{M}_n \dot{\mathbf{Z}}_n - \mathbf{F}^0_n - \mathbf{F}^a_n. \tag{18}$$

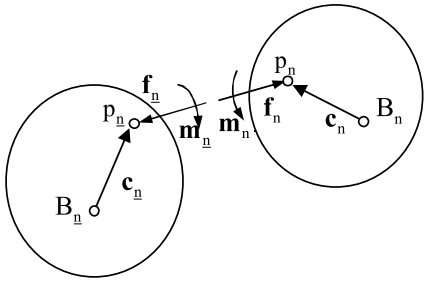

Fig. 2 Reaction forces of the joint connected to the tree-end body

Since joint n is the only joint that connected to the tree-end body n, $\mathbf{F}_n^c$ results solely from the joint reaction force $\mathbf{f}_n$ and torque $\mathbf{m}_n$ of joint n, as shown in Fig. 2. Therefore, the virtual power of $\mathbf{F}_n^c$ is equal to the summary of the virtual power of $\mathbf{f}_n$ and the virtual power of $\mathbf{m}_n$, i.e.,

$$\delta \mathbf{Z}_n^T \mathbf{F}_n^c = \delta \mathbf{v}_{p_n}^T \mathbf{f}_n + \delta \boldsymbol{\omega}_n^T \mathbf{m}_n, \tag{19}$$

where, $\mathbf{v}_{p_n}$ is the velocity of the point p_n, and $\boldsymbol{\omega}_n$ is the angular velocity of the tree-end body n. By the same principle, the virtual power of the joint reaction force $\mathbf{f}_{\underline{n}}$ and torque $\mathbf{m}_{\underline{n}}$ acting at the point $p_{\underline{n}}$ should obey the following equation:

$$\delta \mathbf{Z}_{\underline{n}}^T \mathbf{F}_{n\underline{n}}^c = \delta \mathbf{v}_{p_{\underline{n}}}^T \mathbf{f}_{\underline{n}} + \delta \boldsymbol{\omega}_{\underline{n}}^T \mathbf{m}_{\underline{n}}, \tag{20}$$

where

$$\mathbf{F}_{n\underline{n}}^c = \begin{bmatrix} \mathbf{f}_{\underline{n}} \\ \mathbf{c}_{\underline{n}} \times \mathbf{f}_{\underline{n}} + \mathbf{m}_{\underline{n}} \end{bmatrix}. \tag{21}$$

Assuming that the joint reaction forces are workless, one can conclude that

$$\delta \mathbf{Z}_{\underline{n}}^T \mathbf{F}_{n\underline{n}}^c + \delta \mathbf{Z}_n^T \mathbf{F}_n^c = 0. \tag{22}$$

According to (8), $\delta \mathbf{Z}_n$ can be expressed in terms of $\delta \mathbf{Z}_{\underline{n}}$ and $\delta \dot{\mathbf{q}}_n$. Consequently, (22) can be rewritten as

$$\delta \mathbf{Z}_{\underline{n}}^T \left(\mathbf{F}_{n\underline{n}}^c + \boldsymbol{\Gamma}_n^T \mathbf{F}_n^c \right) + \delta \dot{\mathbf{q}}_n^T \boldsymbol{\Pi}_n^T \mathbf{F}_n^c = 0. \tag{23}$$

Since the variations, $\delta \mathbf{Z}_{\underline{n}}$ and $\delta \dot{\mathbf{q}}_n$ are independent to each other, the corresponding coefficients matrices in (23) must vanish; that is,

$$\boldsymbol{\Pi}_n^T \mathbf{F}_n^c = \mathbf{0}, \tag{24}$$

$$\mathbf{F}_{n\underline{n}}^c = -\boldsymbol{\Gamma}_n^T \mathbf{F}_n^c. \tag{25}$$

Applying of (18) and (14), one can expand (24) as

$$\left(\boldsymbol{\Pi}_n^T \mathbf{M}_n \boldsymbol{\Pi}_n \right) \ddot{\mathbf{q}}_n + \left(\boldsymbol{\Pi}_n^T \mathbf{M}_n \boldsymbol{\Gamma}_n \right) \dot{\mathbf{Z}}_{\underline{n}} - \boldsymbol{\Pi}_n^T \left(\mathbf{F}_n^a + \mathbf{F}_n^0 - \mathbf{M}_n \mathbf{w}_n \right) = \mathbf{0} \tag{26}$$

from which $\ddot{\mathbf{q}}_n$ is solved:

$$\ddot{\mathbf{q}}_n = \mathbf{H}_n^z \dot{\mathbf{Z}}_{\underline{n}} + \mathbf{H}_n^f \mathbf{F}_n^a + \mathbf{y}_n^0, \tag{27}$$

where

$$\mathbf{H}_n^z = -\left(\mathbf{\Pi}_n^T \mathbf{M}_n \mathbf{\Pi}_n\right)^{-1} \left(\mathbf{\Pi}_n^T \mathbf{M}_n \mathbf{\Gamma}_n\right), \tag{28}$$

$$\mathbf{H}_n^f = \left(\mathbf{\Pi}_n^T \mathbf{M}_n \mathbf{\Pi}_n\right)^{-1} \mathbf{\Pi}_n^T, \tag{29}$$

$$\mathbf{y}_n^0 = \left(\mathbf{\Pi}_n^T \mathbf{M}_n \mathbf{\Pi}_n\right)^{-1} \mathbf{\Pi}_n^T \left(\mathbf{F}_n^0 - \mathbf{M}_n \mathbf{w}_n\right). \tag{30}$$

Substituting (27) into (14), results in a new form of recursive kinematical relationship:

$$\dot{\mathbf{Z}}_n = \mathbf{C}_n^z \dot{\mathbf{Z}}_{\underline{n}} + \mathbf{C}_n^f \mathbf{F}_n^a + \mathbf{z}_n^0, \tag{31}$$

where

$$\mathbf{C}_n^z = \mathbf{\Gamma}_n + \mathbf{\Pi}_n \mathbf{H}_n^z, \tag{32}$$

$$\mathbf{C}_n^f = \mathbf{\Pi}_n \mathbf{H}_n^f, \tag{33}$$

$$\mathbf{z}_n^0 = \mathbf{w}_n + \mathbf{\Pi}_n \mathbf{y}_n^0. \tag{34}$$

With the combination of (25), (18), and (31), $\mathbf{F}_{n\underline{n}}^c$ can be formulated as

$$\mathbf{F}_{n\underline{n}}^c = -\left(\Delta \mathbf{M}_{n\underline{n}} \dot{\mathbf{Z}}_{\underline{n}} - \Delta \mathbf{F}_{n\underline{n}}^0 - \Delta \mathbf{F}_{n\underline{n}}^a\right), \tag{35}$$

where

$$\Delta \mathbf{M}_{n\underline{n}} = \mathbf{D}_{n\underline{n}} \mathbf{M}_n \mathbf{\Gamma}_n, \tag{36}$$

$$\Delta \mathbf{F}_{n\underline{n}}^a = \mathbf{D}_{n\underline{n}} \mathbf{F}_n^a, \tag{37}$$

$$\Delta \mathbf{F}_{n\underline{n}}^0 = \mathbf{D}_{n\underline{n}} \left(\mathbf{F}_n^0 - \mathbf{M}_n \mathbf{w}_n\right), \tag{38}$$

$$\mathbf{D}_{n\underline{n}} = \left(\mathbf{C}_n^z\right)^T. \tag{39}$$

Because $\mathbf{F}_{n\underline{n}}^c$ is the generalized interaction force between the tree-end body n and its inboard body $\underline{n}$, the dynamic behavior of the subsystem generated by removing the tree-end body n and applying the force $\mathbf{F}_{n\underline{n}}^c$ on its inboard body $\underline{n}$ is the same as that of its counterpart in the original system. Therefore, as shown in Fig. 3, the system can be reduced to the subsystem in which the tree-end body n and the joint n are removed, as long as the mass matrix of body $\underline{n}$ and the forces acting on body $\underline{n}$ are modified as

$$\bar{\mathbf{M}}_{\underline{n}} = \mathbf{M}_{\underline{n}} + \Delta \mathbf{M}_{n\underline{n}}, \tag{40}$$

$$\bar{\mathbf{F}}_{\underline{n}}^a = \mathbf{F}_{\underline{n}}^a + \Delta \mathbf{F}_{n\underline{n}}^a, \tag{41}$$

$$\bar{\mathbf{F}}_{\underline{n}}^0 = \mathbf{F}_{\underline{n}}^0 + \Delta \mathbf{F}_{n\underline{n}}^0. \tag{42}$$

Being also a system with tree topology, the reduced system can be further reduced to a subsystem with fewer bodies and joints by the application of the described method. In this way, a subsystem with only one body can be obtained. It is worth noting that (40)–(42) have been presented by Featherstone [37, 39] and employed by some other authors [32–36], but they mainly focused on the relevant mathematic procedure.

In the process of system reduction, the mass matrix and the acting forces of each body change at least once and the final values of them are of great physical significance. When

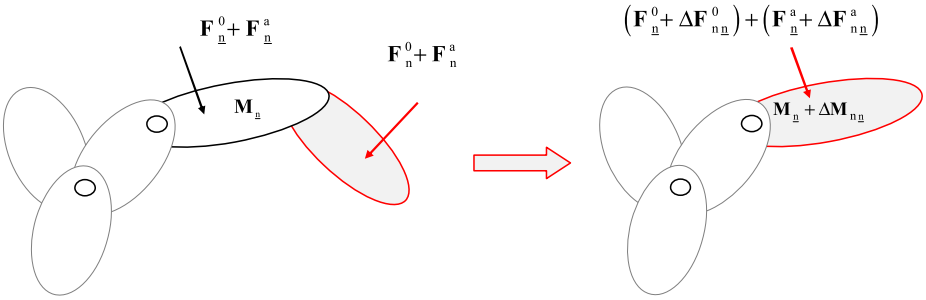

Fig. 3 Decoupling of systems with tree topology

a tree-end body is removed from a multibody system, the motion of the rest of bodies will change in every aspect because of the coupling effect between bodies. From the above analysis, it is seen that the coupling effect can be taken into account explicitly by modifying the mass matrices and the acting forces of the remainder bodies according to (36)–(42). The final values of the modified mass matrix $\bar{\mathbf{M}}_i$ and acting forces $\bar{\mathbf{F}}_i^a$ and $\bar{\mathbf{F}}_i^0$ of body i are the equivalent mass matrix and acting forces that enable the dynamic behavior of the subsystem unchanged, when body i becomes one of the tree-end bodies in the subsystem. The joint reaction force $\mathbf{F}_i^c$ of the joint i can be easily solved from (15) provided the mass matrix, velocity dependent force and applied force are substituted by $\bar{\mathbf{M}}_i$, $\bar{\mathbf{F}}_i^a$, and $\bar{\mathbf{F}}_i^0$, respectively. From this point of view, (36)–(42) should be considered as the rules of inertia and forces transmission, instead of merely as mathematical formulas. It is also noted the matrix $\mathbf{D}_{n\underline{n}}$ in (39) is independent to accelerations and plays an important role in the transmission of inertia and forces.

4 Constraint equations of cut joints

In a multibody system with closed loops, there are multiple choices of joint coordinates. As a common methodology, each closed loop in the system is opened by cutting a joint to construct a system with tree topology and make the system variables clear. The joint coordinates in the generated system are no longer independent to each other, and must obey the cut joint constraint equations which should be generated automatically.

4.1 Rotational constraint equation

The relative rotation between a pair of joint frames associated with a cut joint i, as shown in Fig. 4, can be described in terms of Cardan angles α, β, and γ [38, 39]. Conversely, Cardan angles can be related to the product of two axis vectors of the joint frames in the following way:

$$\mathbf{h}_i^3 \cdot \mathbf{h}_{\underline{i}}^1 = \sin\beta, \tag{43}$$

$$\mathbf{h}_i^2 \cdot \mathbf{h}_{\underline{i}}^1 = -\sin\gamma\cos\beta, \tag{44}$$

$$\mathbf{h}_i^3 \cdot \mathbf{h}_{\underline{i}}^2 = -\sin\alpha\cos\beta. \tag{45}$$

Cardan angles corresponding to the specific joint should satisfy certain conditions. For example, a revolute joint requires that $\beta = 0$ and $\gamma = 0$. This requirement can be represented

Fig. 4 A pair of joint frames

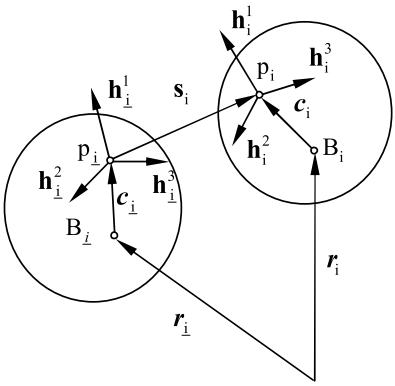

by the equations $\mathbf{h}_{\underline{i}}^3 \cdot \mathbf{h}_i^1 = 0$ and $\mathbf{h}_{\underline{i}}^2 \cdot \mathbf{h}_i^1 = 0$, respectively, in accordance with (43) and (44). Selecting $\mathbf{h}_{\underline{i}}^1$ and $\mathbf{h}_i^2$ as the two rotational axes of a universal joint, one can rewrite the corresponding constraint equation $\gamma = 0$ as $\mathbf{h}_{\underline{i}}^1 \cdot \mathbf{h}_i^2 = 0$. In summary, each rotational constraint equation of a joint takes the form of

$$\mathbf{h}_{\underline{i}}^m \cdot \mathbf{h}_i^k = 0 \quad k, m \in (1, 2, 3). \tag{46}$$

Differentiating (46) with respect to time, results in the corresponding velocity and acceleration constraint equations:

$$(\boldsymbol{\omega}_{\underline{i}} - \boldsymbol{\omega}_i) \cdot \left(\mathbf{h}_{\underline{i}}^m \times \mathbf{h}_i^k\right) = 0, \tag{47}$$

$$(\dot{\boldsymbol{\omega}}_{\underline{i}} - \dot{\boldsymbol{\omega}}_i) \cdot \left(\mathbf{h}_{\underline{i}}^m \times \mathbf{h}_i^k\right) + (\boldsymbol{\omega}_{\underline{i}} - \boldsymbol{\omega}_i) \cdot \left(\left(\boldsymbol{\omega}_{\underline{i}} \times \mathbf{h}_{\underline{i}}^m\right) \times \mathbf{h}_i^k + \mathbf{h}_{\underline{i}}^m \times \left(\boldsymbol{\omega}_i \times \mathbf{h}_i^k\right)\right) = 0, \tag{48}$$

where $\boldsymbol{\omega}_{\underline{i}}$ and $\boldsymbol{\omega}_i$ are the angular velocities of the two bodies linked by the cut joint i, as shown in Fig. 4.

4.2 Translational constraint equations

Generally, joint translational axes can be assigned among the axes of joint frames. As an example, $\mathbf{h}_{\underline{i}}^1$ is usually selected as the translational axis vector of a prismatic joint. Therefore, each translational constraint equation can be expressed as

$$(\mathbf{r}_{p_i} - \mathbf{r}_{p_{\underline{i}}}) \cdot \mathbf{h}_{\underline{i}}^k = 0, \tag{49}$$

where $\mathbf{r}_{p_{\underline{i}}} = \mathbf{r}_{\underline{i}} + c_{\underline{i}}$, $\mathbf{r}_{p_i} = \mathbf{r}_i + c_i$ and the vector $\mathbf{h}_{\underline{i}}^k$ is perpendicular to the sliding axis vectors of joint i. The associated velocity and acceleration constraints are given by

$$(\dot{\mathbf{r}}_{p_i} - \dot{\mathbf{r}}_{p_{\underline{i}}}) \cdot \mathbf{h}_{\underline{i}}^k + \boldsymbol{\omega}_{\underline{i}} \cdot \left(\mathbf{h}_{\underline{i}}^k \times (\mathbf{r}_{p_i} - \mathbf{r}_{p_{\underline{i}}})\right) = 0, \tag{50}$$

$$\begin{aligned}(\ddot{\mathbf{r}}_{p_i} - \ddot{\mathbf{r}}_{p_{\underline{i}}}) \cdot \mathbf{h}_i^k + \dot{\boldsymbol{\omega}}_{\underline{i}} \cdot \left(\mathbf{h}_{\underline{i}}^k \times (\mathbf{r}_{p_i} - \mathbf{r}_{p_{\underline{i}}})\right) + 2(\dot{\mathbf{r}}_{p_i} - \dot{\mathbf{r}}_{p_{\underline{i}}}) \cdot \left(\boldsymbol{\omega}_{\underline{i}} \times \mathbf{h}_{\underline{i}}^k\right) \\ + (\mathbf{r}_{p_i} - \mathbf{r}_{p_{\underline{i}}}) \cdot \left(\boldsymbol{\omega}_{\underline{i}} \times \left(\boldsymbol{\omega}_{\underline{i}} \times \mathbf{h}_{\underline{i}}^k\right)\right) = 0,\end{aligned} \tag{51}$$

where the velocity of joint definition points can be expressed as

$$\dot{\mathbf{r}}_{p_{\underline{i}}} = \dot{\mathbf{r}}_{\underline{i}} - \mathbf{c}_{\underline{i}} \times \boldsymbol{\omega}_{\underline{i}}, \tag{52}$$

$$\dot{\mathbf{r}}_{p_i} = \dot{\mathbf{r}}_i - \mathbf{c}_i \times \boldsymbol{\omega}_i \tag{53}$$

and the acceleration of joint definition points can be formulated as

$$\ddot{\mathbf{r}}_{p_{\underline{i}}} = \ddot{\mathbf{r}}_{\underline{i}} - \mathbf{c}_{\underline{i}} \times \dot{\boldsymbol{\omega}}_{\underline{i}} + \boldsymbol{\omega}_{\underline{i}} \times (\boldsymbol{\omega}_{\underline{i}} \times \mathbf{c}_{\underline{i}}), \tag{54}$$

$$\ddot{\mathbf{r}}_{p_i} = \ddot{\mathbf{r}}_i - \mathbf{c}_i \times \dot{\boldsymbol{\omega}}_i + \boldsymbol{\omega}_i \times (\boldsymbol{\omega}_i \times \mathbf{c}_i). \tag{55}$$

In summary, acceleration constraint equations of the joint i can be written in matrix form:

$$\sum_{k=1}^{n} \mathbf{G}_{ik} \dot{\mathbf{Z}}_k + \boldsymbol{\xi}_i = \mathbf{0}, \tag{56}$$

where the coefficient matrices $\mathbf{G}_{ik}$ and vector $\boldsymbol{\xi}_i$ are defined by (51), (54), and (55). They are independent of accelerations.

As compared with that in the traditional form [38, 39], the joint constraint equations expressed in terms of axes of the joint frames, as proposed in this paper, are more convenient to be generated in a programmable manner.

5 Joint reaction forces of frictional joints

When body $\underline{i}$ and body i are linked by a joint i as shown in Fig. 4, the joint exerts joint reaction force $\mathbf{f}_{\underline{i}}$ and torque $\mathbf{m}_{\underline{i}}$ at the inner joint definition point $p_{\underline{i}}$ on body $\underline{i}$ as well as joint reaction force $\mathbf{f}_i$ and torque $\mathbf{m}_i$ at the outer joint definition point p_i on body i. It is a misunderstanding that those reaction forces are the contact forces acting at the joint definition points. One of the reasons is that the joint definition points are not necessarily contact points. For example, the two definition points of a prismatic joint are not coincident in position. In general, body i and its inboard body $\underline{i}$ can be in mutual contact which result in two systems of contact forces acting at many pairs of points on the contiguous bodies.

To avoid ambiguousness, joint reaction force $\mathbf{f}_{\underline{i}}$ and torque $\mathbf{m}_{\underline{i}}$ should be understood as a force system that is equivalent to the contact force system imposed on the body $\underline{i}$; meanwhile the joint reaction force $\mathbf{f}_i$ and torque $\mathbf{m}_i$ should be understood as a force system that is equivalent to the contact force system imposed on the body i. Since the resultant of the two contact force systems are in equilibrium, the resultant of forces $\mathbf{f}_{\underline{i}}$ and $\mathbf{f}_i$ as well as torques $\mathbf{m}_{\underline{i}}$ and $\mathbf{m}_i$ should be in equilibrium; that is to say

$$\mathbf{f}_{\underline{i}} = -\mathbf{f}_i, \tag{57}$$

$$\mathbf{m}_{\underline{i}} = -\mathbf{m}_i - \mathbf{s}_i \times \mathbf{f}_i, \tag{58}$$

where $\mathbf{s}_i$ is the vector of the point p_i relative to the point $p_{\underline{i}}$, as indicated in Fig. 4. Due to the joint constraint, the relative translation and rotation between body $\underline{i}$ and body i must be confined to the subspace S_T and S_R respectively, where S_T is the linear span of translational axis vectors of the joint and S_R is the linear span of rational axis vectors of the joint. We assume that the rotational center of the joint is at the point p_i. In this case, joint reaction force $\mathbf{f}_i$ can be divided into two parts: $\mathbf{f}_i^n$ the force that is perpendicular to the subspace S_T and $\mathbf{f}_i^t$ the force that belongs to the subspace S_T. For example,

$$\mathbf{f}_i^n = \begin{cases} \mathbf{h}_{\underline{i}}^1 \lambda_1 + \mathbf{h}_{\underline{i}}^2 \lambda_2 + \mathbf{h}_{\underline{i}}^3 \lambda_3 & \text{for revolute, universal and spherical joints,} \\ \mathbf{h}_{\underline{i}}^2 \lambda_1 + \mathbf{h}_{\underline{i}}^3 \lambda_2 & \text{for cylindrical and prismatic joints,} \end{cases} \tag{59}$$

$$\mathbf{f}_i^t = \begin{cases} \mathbf{0} & \text{for revolute, universal and spherical joints,} \\ \mathbf{h}_{\underline{i}}^1 \eta_1 & \text{for cylindrical and prismatic joints,} \end{cases} \tag{60}$$

where λ_k and η_k are multipliers representing the magnitudes of forces. In the same manner, joint reaction torque $\mathbf{m}_i$ can be written as $\mathbf{m}_i = \mathbf{m}_i^n + \mathbf{m}_i^t$, where $\mathbf{m}_i^n$ is perpendicular to the subspace S_R and $\mathbf{m}_i^t$ belongs to the subspace S_R. For example,

$$\mathbf{m}_i^n = \begin{cases} \mathbf{0} & \text{for spherical joints,} \\ \mathbf{h}_{\underline{i}}^2 \bar{\lambda}_1 + \mathbf{h}_{\underline{i}}^3 \bar{\lambda}_2 & \text{for cylindrical and revolute joints,} \\ \mathbf{h}_{\underline{i}}^1 \times \mathbf{h}_i^2 \bar{\lambda}_1 & \text{for universal joints,} \\ \mathbf{h}_{\underline{i}}^1 \bar{\lambda}_1 + \mathbf{h}_{\underline{i}}^2 \bar{\lambda}_2 + \mathbf{h}_{\underline{i}}^3 \bar{\lambda}_3 & \text{for prismatic joints,} \end{cases} \tag{61}$$

$$\mathbf{m}_i^t = \begin{cases} \mathbf{h}_{\underline{i}}^1 \bar{\eta}_1 + \mathbf{h}_{\underline{i}}^2 \bar{\eta}_2 + \mathbf{h}_{\underline{i}}^3 \bar{\eta}_3 & \text{for spherical joints,} \\ \mathbf{h}_{\underline{i}}^1 \bar{\eta}_1 & \text{for cylindrical and revolute joints,} \\ \mathbf{h}_{\underline{i}}^1 \bar{\eta}_1 + \mathbf{h}_i^2 \bar{\eta}_2 & \text{for universal joints,} \\ \mathbf{0} & \text{for prismatic joints.} \end{cases} \tag{62}$$

In accordance with (57) and (58), joint reaction force $\mathbf{f}_{\underline{i}}$ and torque $\mathbf{m}_{\underline{i}}$ can be also divided into two parts

$$\mathbf{f}_{\underline{i}}^n = -\mathbf{f}_i^n, \tag{63}$$

$$\mathbf{f}_{\underline{i}}^t = -\mathbf{f}_i^t, \tag{64}$$

$$\mathbf{m}_{\underline{i}}^n = -\mathbf{m}_i^n - \mathbf{s}_i \times \mathbf{f}_i^n, \tag{65}$$

$$\mathbf{m}_{\underline{i}}^t = -\mathbf{m}_i^t - \mathbf{s}_i \times \mathbf{f}_i^t. \tag{66}$$

As a whole, reaction forces of joint i can be taken as a force system made up of two parts. The first part consists of forces $\mathbf{f}_i^n$ and $\mathbf{f}_{\underline{i}}^n$ together with torques $\mathbf{m}_i^n$ and $\mathbf{m}_{\underline{i}}^n$ and the second part consists of forces $\mathbf{f}_i^t$ and $\mathbf{f}_{\underline{i}}^t$ together with torques $\mathbf{m}_i^t$ and $\mathbf{m}_{\underline{i}}^t$. The virtual power of the first part is

$$\delta p_i^n = \delta \bar{\mathbf{v}}_i^T \mathbf{f}_i^n + \delta \bar{\boldsymbol{\omega}}_i^T \mathbf{m}_i^n, \tag{67}$$

where the joint angular velocity is $\bar{\boldsymbol{\omega}}_i = \mathbf{P}_i^r \dot{\mathbf{q}}_i$ and the joint relative sliding velocity is

$$\bar{\mathbf{v}}_i = \mathbf{v}_{p_i} - \mathbf{v}_{p_{\underline{i}}} - \boldsymbol{\omega}_{\underline{i}} \times \mathbf{s}_i = \mathbf{P}_i^s \dot{\mathbf{q}}_i. \tag{68}$$

Since $\bar{\mathbf{v}}_i$ and $\bar{\boldsymbol{\omega}}_i$ are perpendicular to the joint reaction force $\mathbf{f}_i^n$ and torque $\mathbf{m}_i^n$, respectively, the virtual power $\delta p_i^n = 0$ which means that the first part of the joint reaction forces is workless. The virtual power of the second part

$$\delta p_i^t = \delta \bar{\mathbf{v}}_i^T \mathbf{f}_i^t + \delta \bar{\boldsymbol{\omega}}_i^T \mathbf{m}_i^t. \tag{69}$$

It is seen from (69) that δp_i^t is not necessarily zero if $\mathbf{f}_{i-}^t$ and torque $\mathbf{m}_{i-}^t$ do not vanish. Therefore, the second part of joint reaction forces results from friction and should be treated as applied forces.

When joint i is cut off to form a system with tree topology, the joint reaction forces are treated as applied forces. The generalized force $\mathbf{N}_i$ on body i caused by $\mathbf{f}_i$ and $\mathbf{m}_i$ can be solved from the following virtual power equation

$$\delta \mathbf{v}_p^T \mathbf{f}_i + \delta \boldsymbol{\omega}_i^T \mathbf{m}_i = \delta \mathbf{Z}_i^T \mathbf{N}_i. \tag{70}$$

By substituting (59)–(62) into (70), one can obtain that

$$\mathbf{N}_i = \hat{\mathbf{W}}_i^N \boldsymbol{\lambda}_i + \hat{\mathbf{W}}_i^F \boldsymbol{\eta}_i. \tag{71}$$

In the same manner, the generalized force $\mathbf{N}_{\underline{i}}$ on body $\underline{i}$ caused by $\mathbf{f}_{\underline{i}}$ and $\mathbf{m}_{\underline{i}}$ can be written as

$$\mathbf{N}_{\underline{i}} = \hat{\mathbf{W}}_{\underline{i}}^N \boldsymbol{\lambda}_i + \hat{\mathbf{W}}_{\underline{i}}^F \boldsymbol{\eta}_i. \tag{72}$$

In (71) and (72), the coefficient matrices $\hat{\mathbf{W}}_i^N$, $\hat{\mathbf{W}}_i^F$, $\hat{\mathbf{W}}_{\underline{i}}^N$, and $\hat{\mathbf{W}}_{\underline{i}}^F$ are independent of system accelerations but dependent on the type of the joint.

6 Recursive formulations of general multibody systems

A multibody system with frictional joints can be regarded as an ideal system as long as frictional forces and torques are treated as applied forces, and a multibody system with closed loops can be transformed into a system with tree topology if joint reaction forces and torques of the cut joints are regarded as applied forces, as shown in Fig. 5.

Based on (71) and (72), the augmented external forces on body i can be expressed in the form as follows:

$$\bar{\mathbf{F}}_i^a = \mathbf{F}_i^a + \mathbf{W}_i^N \boldsymbol{\lambda} + \mathbf{W}_i^F \boldsymbol{\eta}. \tag{73}$$

Accordingly, (27) and (31) are rewritten as

$$\ddot{\mathbf{q}}_n = \mathbf{H}_n^z \dot{\mathbf{Z}}_{\underline{n}} + \mathbf{H}_n^\lambda \boldsymbol{\lambda} + \mathbf{H}_n^\eta \boldsymbol{\eta} + \bar{\mathbf{y}}_n^0, \tag{74}$$

$$\dot{\mathbf{Z}}_n = \mathbf{C}_n^z \dot{\mathbf{Z}}_{\underline{n}} + \mathbf{C}_n^\lambda \boldsymbol{\lambda} + \mathbf{C}_n^\eta \boldsymbol{\eta} + \bar{\mathbf{z}}_n^0, \tag{75}$$

where

$$\mathbf{H}_n^\lambda = \mathbf{H}_n^f \mathbf{W}_n^N; \qquad \mathbf{H}_n^\eta = \mathbf{H}_n^f \mathbf{W}_n^F; \qquad \bar{\mathbf{y}}_n^0 = \mathbf{y}_n^0 + \mathbf{H}_n^f \mathbf{F}_n^a, \tag{76}$$

$$\mathbf{C}_n^\lambda = \mathbf{C}_n^f \mathbf{W}_n^N; \qquad \mathbf{C}_n^\eta = \mathbf{C}_n^f \mathbf{W}_n^F; \qquad \bar{\mathbf{z}}_n^0 = \mathbf{z}_n^0 + \mathbf{C}_n^f \mathbf{F}_n^a. \tag{77}$$

By replacing the original external force $\mathbf{F}_i^a$ with the augmented external force $\bar{\mathbf{F}}_i^a$, the transmission of inertias and forces of a multibody system with frictional joints and closed loops can be carried out by the method as introduced in Sect. 3. According to (37), when the tree-end body n is removed, coefficient matrices $\mathbf{W}_{\underline{n}}^N$ and $\mathbf{W}_{\underline{n}}^F$ of its inboard body $\underline{n}$ should be modified as

$$\bar{\mathbf{W}}_{\underline{n}}^N = \mathbf{W}_{\underline{n}}^N + \mathbf{D}_{n\underline{n}} \mathbf{W}_n^N, \tag{78}$$

$$\bar{\mathbf{W}}_{\underline{n}}^F = \mathbf{W}_{\underline{n}}^F + \mathbf{D}_{n\underline{n}} \mathbf{W}_n^F. \tag{79}$$

Recursive application of the method for decoupling an ideal system with tree topology can finally yield a reduced system with only one body. Its equation of motion can be written in the form as

$$\ddot{\mathbf{q}}_1 = \mathbf{H}_1^\lambda \boldsymbol{\lambda} + \mathbf{H}_1^\eta \boldsymbol{\eta} + \mathbf{y}_0, \tag{80}$$

where

$$\mathbf{y}_0 = \mathbf{H}_1^z \dot{\mathbf{Z}}_0 + \bar{\mathbf{y}}_1^0. \tag{81}$$

However, more equations are required to determine the multipliers $\boldsymbol{\lambda}$ and $\boldsymbol{\eta}$.

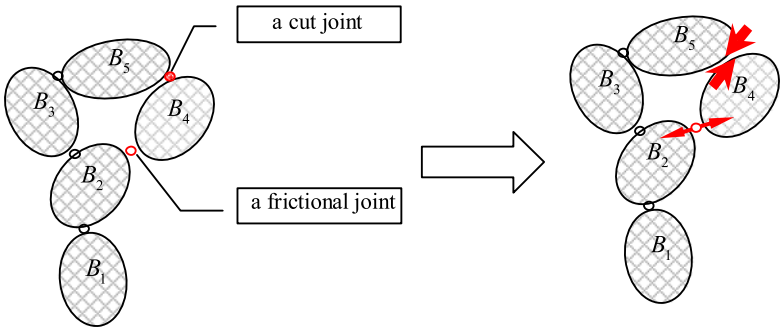

Fig. 5 Equivalence between general systems and ideal systems with tree topology

Partial equations are supplied by the constraint equations of closed loops. Initially, these constraint equations can be formulated in the following form:

$$\sum_{k=1}^{n} \mathbf{G}_k \dot{\mathbf{Z}}_k + \mathbf{G}_\lambda \boldsymbol{\lambda} + \mathbf{G}_\eta \boldsymbol{\eta} + \boldsymbol{\xi} = \mathbf{0}, \tag{82}$$

where $\mathbf{G}_\lambda$ and $\mathbf{G}_\eta$ are zero matrices in accordance with (56). By means of (75), $\dot{\mathbf{Z}}_n$ can be removed from (82), provided the coefficient matrices are modified as

$$\mathbf{G}_{\underline{n}} = \mathbf{G}_{\underline{n}} + \mathbf{G}_n \mathbf{C}_n^z, \tag{83}$$

$$\mathbf{G}_\lambda = \mathbf{G}_\lambda + \mathbf{G}_n \mathbf{C}_n^f \mathbf{W}_n^N, \tag{84}$$

$$\mathbf{G}_\eta = \mathbf{G}_\eta + \mathbf{G}_n \mathbf{C}_n^f \mathbf{W}_n^F, \tag{85}$$

$$\boldsymbol{\xi} = \boldsymbol{\xi} + \mathbf{G}_n \left(\mathbf{z}_n^0 + \mathbf{C}_n^f \mathbf{F}_n^a \right). \tag{86}$$

From now on, matrices $\mathbf{G}_\lambda$ and $\mathbf{G}_\eta$ become nonzero. In the same manner, all terms of $\dot{\mathbf{Z}}_k$ with $k > 1$ can be eliminated from (82) recursively while $\mathbf{G}_\lambda$, $\mathbf{G}_\eta$, $\mathbf{G}_k$, and $\boldsymbol{\xi}$ change according to (83)–(86). Finally, the constraint equations can be converted into the form as

$$\mathbf{G}_1 \dot{\mathbf{Z}}_1 + \mathbf{G}_\lambda \boldsymbol{\lambda} + \mathbf{G}_\eta \boldsymbol{\eta} + \boldsymbol{\xi} = \mathbf{0}. \tag{87}$$

Considering (14), this equation can be rewritten as

$$\mathbf{G}_q \ddot{\mathbf{q}}_1 + \mathbf{G}_\lambda \boldsymbol{\lambda} + \mathbf{G}_\eta \boldsymbol{\eta} + \boldsymbol{\xi}_0 = \mathbf{0}, \tag{88}$$

where

$$\mathbf{G}_q = \mathbf{G}_1 \boldsymbol{\Pi}_1; \qquad \boldsymbol{\xi}_0 = \boldsymbol{\xi} + \mathbf{G}_1 (\boldsymbol{\Gamma}_1 \dot{\mathbf{Z}}_0 + \mathbf{w}_1). \tag{89}$$

From (80) and (88), multipliers $\boldsymbol{\lambda}$ can be solved as

$$\boldsymbol{\lambda} = \boldsymbol{\lambda}_0 + \mathbf{S}_\lambda \boldsymbol{\eta}, \tag{90}$$

where

$$\boldsymbol{\lambda}_0 = -\left(\mathbf{G}_\lambda + \mathbf{G}_q \mathbf{H}_1^\lambda \right)^{-1} (\mathbf{G}_q \mathbf{y}_0 + \boldsymbol{\xi}_0), \tag{91}$$

$$\mathbf{S}_\lambda = -\left(\mathbf{G}_\lambda + \mathbf{G}_q \mathbf{H}_1^\lambda \right)^{-1} \left(\mathbf{G}_\eta + \mathbf{G}_q \mathbf{H}_1^\eta \right). \tag{92}$$

Substituting (90) into (80) yields

$$\ddot{\mathbf{q}}_1 = \mathbf{a}_1^q + \mathbf{A}_1^q \boldsymbol{\eta}, \tag{93}$$

where

$$\mathbf{a}_1^q = \mathbf{y}_0 + \mathbf{H}_1^{\lambda} \boldsymbol{\lambda}_0, \tag{94}$$

$$\mathbf{A}_1^q = \mathbf{H}_1^{\eta} + \mathbf{H}_1^{\lambda} \mathbf{S}_{\lambda}. \tag{95}$$

Based on (74) and (75), accelerations $\dot{\mathbf{Z}}_i$ and $\ddot{\mathbf{q}}_i$ can be written in the form

$$\dot{\mathbf{Z}}_i = \mathbf{a}_i^z + \mathbf{A}_i^z \boldsymbol{\eta}, \tag{96}$$

$$\ddot{\mathbf{q}}_i = \mathbf{a}_i^q + \mathbf{A}_i^q \boldsymbol{\eta}, \tag{97}$$

where the coefficient matrices in the above two equations are obtained in a recursive manner as follows:

$$\mathbf{a}_1^z = \mathbf{C}_1^z \dot{\mathbf{Z}}_0 + \mathbf{C}_1^{\lambda} \boldsymbol{\lambda}_0 + \bar{\mathbf{z}}_1^0; \qquad \mathbf{A}_1^z = \mathbf{C}_1^{\lambda} \mathbf{S}_{\lambda} + \mathbf{C}_1^{\eta}, \tag{98}$$

$$\mathbf{a}_2^q = \mathbf{H}_2^z \mathbf{a}_1^z + \mathbf{H}_2^{\lambda} \boldsymbol{\lambda}_0 + \bar{\mathbf{y}}_2^0; \qquad \mathbf{A}_2^q = \mathbf{H}_2^z \mathbf{A}_1^z + \mathbf{H}_2^{\lambda} \mathbf{S}_{\lambda} + \mathbf{H}_2^{\eta}, \tag{99}$$

$$\cdots$$

$$\mathbf{a}_i^z = \mathbf{C}_i^z \mathbf{a}_{\underline{i}}^z + \mathbf{C}_i^{\lambda} \boldsymbol{\lambda}_0 + \bar{\mathbf{z}}_i^0; \qquad \mathbf{A}_i^z = \mathbf{C}_i^z \mathbf{A}_{\underline{i}}^z + \mathbf{C}_i^{\lambda} \mathbf{S}_{\lambda} + \mathbf{C}_i^{\eta}, \tag{100}$$

$$\mathbf{a}_{i+1}^q = \mathbf{H}_{i+1}^z \mathbf{a}_{i+1}^z + \mathbf{H}_{i+1}^{\lambda} \boldsymbol{\lambda}_0 + \bar{\mathbf{y}}_{i+1}^0; \qquad \mathbf{A}_{i+1}^q = \mathbf{H}_{i+1}^z \mathbf{A}_{i+1}^z + \mathbf{H}_{i+1}^{\lambda} \mathbf{S}_{\lambda} + \mathbf{H}_{i+1}^{\eta}, \tag{101}$$

$$\cdots$$

$$\mathbf{a}_n^q = \mathbf{H}_n^z \mathbf{a}_{\underline{n}}^z + \mathbf{H}_n^{\lambda} \boldsymbol{\lambda}_0 + \bar{\mathbf{y}}_n^0; \qquad \mathbf{A}_n^q = \mathbf{H}_n^z \mathbf{A}_{\underline{n}}^z + \mathbf{H}_n^{\lambda} \mathbf{S}_{\lambda} + \mathbf{H}_n^{\eta}. \tag{102}$$

In the case that the frictional joint is a cut joint, all the associated joint reaction forces have been expressed as the function of multipliers $\boldsymbol{\eta}$ as shown by (59)–(62) and (90). In the case that the frictional joint i is not a cut joint, the frictional forces are formulated by (60) and (62). Meanwhile, its workless part of joint reaction forces can be given by

$$\mathbf{N}_i^N = \mathbf{M}_i \dot{\mathbf{Z}}_i - \left(\mathbf{F}_i^0 + \mathbf{F}_i^a + \mathbf{W}_i^N \boldsymbol{\lambda} + \mathbf{W}_i^F \boldsymbol{\eta}\right). \tag{103}$$

It should be noted that the mass matrix, forces and coefficient matrices at the right side of (103) must be evaluated under the condition that body i becomes a tree-end body in one of the reduced systems given by the decoupling procedure described in Sect. 3. Substituting (90) and (96) into (103), one can express $\mathbf{N}_i^N$ as the linear function of $\boldsymbol{\eta}$.

A group of complement equations for solving multipliers $\boldsymbol{\eta}$ are necessary to complete the solutions. As shown in the following section, these equations are usually nonlinear with respect to $\boldsymbol{\eta}$. They can be solved by a suitable equation solver such as FSOLVE in the Matlab.

7 Non-colliding contact analysis of joints

Contact analysis varies with the type and geometry of joints and depends on the friction model. Coulomb dry friction model is most frequently used partly because of its simplicity in the expression. However, its application in multibody systems usually involves many difficult problems. For example, when the relative velocity between a mating pair is zero,

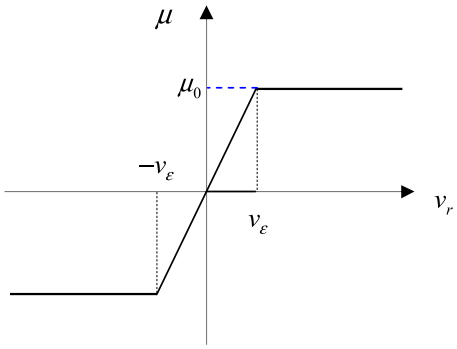

Fig. 6 Rooney and Deravi friction model; v_r—Relative velocity; μ—Friction coefficient

the friction force should be evaluated in the following manner. A constraint of the relative acceleration being zero is temporarily imposed on the system, and the friction force is calculated accordingly. If the obtained friction force is greater than the static friction force, then the constraint is released and the friction force is evaluated under this new condition. Combinatorial problems and switching between sticking and sliding phase involved in such a procedure may lead to great numerical difficulties. From a mathematical point of view, Coulomb friction force is a set value function of sliding velocity [40], and its application may result in non-uniqueness and nonexistence of solutions according to the theory of non-smooth analysis [41]. On the other hand, it is revealed by the modern tribology that discontinuity of friction force is not a physical fact [42]. Instead of the Coulomb's friction law, some smooth friction models can be used. Pennestri, Valentini and Vita [42] presented the application of the Dahl friction model in planar multibody systems, but the model is too complicated for general multibody systems.

In this paper, a simple continuous friction model:

$$\mu = \begin{cases} \mu_0, & |v_r| \geq v_\varepsilon, \\ \frac{|v_r|}{v_\varepsilon}\mu_0, & |v_r| < v_\varepsilon \end{cases} \tag{104}$$

proposed by Rooney and Deravi [43] is adopted. As qualitatively illustrated in Fig. 6, this model can greatly weaken the negative effect of sticking-sliding switch, at the cost that zero friction force is predicted at the zero relative velocity. If no adhesion between any mating pair is maintained for a long time, this model is acceptable in practice.

Although the effects of collisions are assumed to be negligible, joint clearances are taken in to account qualitatively in this paper. In fact, joint clearances are necessary to enable relative movements. Due to clearances, no joint can make its designed kinematic constraint perfectly. But they are usually kept under control by the construction of joints to restrict the undesired relative motion. In this paper, we assume that joint clearances exist but are infinitely small. In this case, constraint violations and collisions are negligible, but contact forces and contact positions still play an important role in the formulation of frictional forces. In order to describe positions of possible contact points, a group of parameters, such as the normal vector at the contact point on the ball of a spherical joint, the two orientation angles of the contact points on the lateral surface of the shaft of a cylindrical joint, etc., are introduced depending on the type of joints. These parameters cannot be evaluated in terms of joint coordinates since they are compatible with joint constraints. However, they are closely related to the joint reaction forces. Based on such kind of relations, equations for multipliers $\boldsymbol{\eta}$ can be given. Moreover, locations of contact points and associated contact forces can also be obtained, as shown in the following sections.

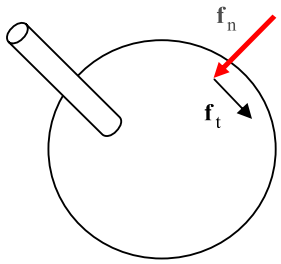

Fig. 7 Contact in a spherical joint

7.1 Spherical joints

A spherical joint consists of a socket and a ball. As illustrated in Fig. 7, on the ball there is only one possible contact point, and the normal contact force exerted on the ball can be written as

$$\mathbf{f}_n = -f_n \mathbf{n}, \tag{105}$$

where f_n is the norm of $\mathbf{f}_n$ and $\mathbf{n}$ is the unit outward normal vector at the contact point. Without loss of generality, the ball is assumed to be fixed on the inboard body of the joint. As a result, the relative angular velocity of the ball with respect to the socket is equal and opposite to the joint angular velocity $\boldsymbol{\omega}_r$, and the relative velocity of the contact point with respect to the socket is written as

$$\mathbf{v}_r = -r\boldsymbol{\omega}_r \times \mathbf{n}, \tag{106}$$

where r is the radius of the ball. Based on the Coulomb law of friction, the frictional force exerted on the ball is given by

$$\mathbf{f}_t = kf\boldsymbol{\omega}_r \times \mathbf{n}, \tag{107}$$

where

$$k = \frac{\mu}{\|\boldsymbol{\omega}_r \times \mathbf{n}\|} = \frac{\mu}{\sqrt{\boldsymbol{\omega}_r \cdot \boldsymbol{\omega}_r - (\boldsymbol{\omega}_r \cdot \mathbf{n})^2}} \tag{108}$$

and μ is the coefficient of friction. Because the contact force system is statically equivalent to the joint reaction force system, the joint reaction force $\mathbf{f}_c$ and torque $\mathbf{m}_c$ at the center of the ball can be formulated as

$$\mathbf{f}_c = f_n(k\boldsymbol{\omega}_r \times \mathbf{n} - \mathbf{n}), \tag{109}$$

$$\mathbf{m}_c = rf_n\mathbf{n} \times (k\boldsymbol{\omega}_r \times \mathbf{n}). \tag{110}$$

From (109), the magnitude of the normal contact force is solved:

$$f_n = \sqrt{\frac{\mathbf{f}_c \cdot \mathbf{f}_c}{1+\mu^2}} \tag{111}$$

and the dot product of $\mathbf{f}_c$ and $\boldsymbol{\omega}_r$ is given by

$$\mathbf{f}_c \cdot \boldsymbol{\omega}_r = -f\boldsymbol{\omega}_r \cdot \mathbf{n}. \tag{112}$$

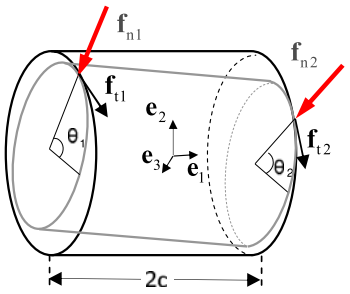

Fig. 8 Contacts in a cylindrical joint

Substitution of (112) into (108) yields

$$k = \frac{f_n \mu}{\sqrt{f_n^2 \boldsymbol{\omega}_r \cdot \boldsymbol{\omega}_r - (\mathbf{f}_c \cdot \boldsymbol{\omega}_r)^2}}. \tag{113}$$

Rewriting (109) in matrix form, one can obtain

$$\mathbf{n} = \frac{1}{f_n}(k\tilde{\boldsymbol{\omega}}_r - \mathbf{E})^{-1}\mathbf{f}_c, \tag{114}$$

where $\mathbf{E}$ is the 3×3 unit matrix. It is seen from (111), (113), and (114) the outward normal vector at the contact point can be formulated in terms of the joint reaction force $\mathbf{f}_c$.

In summary, both of the location and the forces of the contact in a spherical joint can be fully determined by the joint reaction force $\mathbf{f}_c$ which is the known function of the multipliers $\boldsymbol{\eta}$ as shown by (103). As a result, (110) implies something new about the multipliers $\boldsymbol{\eta}$, and is just the required complement equation for spherical joints. Since f_n is a nonlinear function of $\mathbf{f}_c$, the complement equation is nonlinear with respective to the multipliers $\boldsymbol{\eta}$.

7.2 Cylindrical joints

A cylindrical joint consists of a guide and a shaft. On the shaft, there are two possible contact points, as illustrated in Fig. 8 where θ_1 and θ_2 are orientation angles of the contact points respectively, and $2c$ is the length of the shaft. We also assume that the shaft is fixed on the inboard body of the joint.

The relative velocities of the contact points with respect to the guide can be formulated in terms of the joint angular velocity $\omega_r \mathbf{e}_1$ and sliding velocity $\dot{s}\mathbf{e}_1$ as follows:

$$\mathbf{v}_1 = -\dot{s}\mathbf{e}_1 - \omega_r \mathbf{e}_1 \times r(\cos\theta_1 \mathbf{e}_3 + \sin\theta_1 \mathbf{e}_2), \tag{115}$$

$$\mathbf{v}_2 = -\dot{s}\mathbf{e}_1 - \omega_r \mathbf{e}_1 \times r(\cos\theta_2 \mathbf{e}_3 + \sin\theta_2 \mathbf{e}_2), \tag{116}$$

where r is the radius of the shaft. The normal contact forces exerted on the shaft can be expressed in terms of their magnitudes f_1 and f_2 as

$$\mathbf{f}_{n1} = -f_1 \cos\theta_1 \mathbf{e}_3 - f_1 \sin\theta_1 \mathbf{e}_2, \tag{117}$$

$$\mathbf{f}_{n2} = -f_2 \cos\theta_2 \mathbf{e}_3 - f_2 \sin\theta_2 \mathbf{e}_2, \tag{118}$$

where f_1 and f_2 must be positive in order to make the orientation angles unambiguous. According to the Coulomb law of friction, the corresponding frictional forces can be written

as

$$\mathbf{f}_{t1} = f_1(k_s\mathbf{e}_1 - k_r\cos\theta_1\mathbf{e}_2 + k_r\sin\theta_1\mathbf{e}_3), \tag{119}$$

$$\mathbf{f}_{t2} = f_2(k_s\mathbf{e}_1 - k_r\cos\theta_2\mathbf{e}_2 + k_r\sin\theta_2\mathbf{e}_3), \tag{120}$$

where

$$k_r = \frac{\mu\omega_r r}{\sqrt{\dot{s}^2 + \omega_r^2 r^2}}; \qquad k_s = \frac{\mu\dot{s}}{\sqrt{\dot{s}^2 + \omega_r^2 r^2}}. \tag{121}$$

The reaction force and torque at the shaft center, expressed as $\mathbf{f}_c = f_{c1}\mathbf{e}_1 + f_{c2}\mathbf{e}_2 + f_{c3}\mathbf{e}_3$ and $\mathbf{m}_c = m_{c1}\mathbf{e}_1 + m_{c2}\mathbf{e}_2 + m_{c3}\mathbf{e}_3$, respectively, form a force system that is statically equivalent to the contact force system; that is,

$$\mathbf{f}_c = \mathbf{f}_{t1} + \mathbf{f}_{t2} + \mathbf{f}_{n1} + \mathbf{f}_{n2}, \tag{122}$$

$$\mathbf{m}_c = (r\cos\theta_1\mathbf{e}_3 + r\sin\theta_1\mathbf{e}_2 - c\mathbf{e}_1) \times (\mathbf{f}_{n1} + \mathbf{f}_{t1}) + (r\cos\theta_2\mathbf{e}_3 + r\sin\theta_2\mathbf{e}_2 + c\mathbf{e}_1) \times (\mathbf{f}_{n2} + \mathbf{f}_{t2}). \tag{123}$$

In scalar form, they are six equations, and four of them can be rewritten in matrix form as

$$\begin{pmatrix} f_{c2} \\ f_{c3} \\ m_{c2} \\ m_{c3} \end{pmatrix} = \begin{bmatrix} -k_r & -1 & -k_r & -1 \\ -1 & k_r & -1 & k_r \\ k_s r - c & k_r c & c + k_s r & -k_r c \\ k_r c & c - k_s r & -k_r c & -k_s r - c \end{bmatrix} \begin{pmatrix} f_1\cos\theta_1 \\ f_1\sin\theta_1 \\ f_2\cos\theta_2 \\ f_2\sin\theta_2 \end{pmatrix} \tag{124}$$

from which, f_1 and f_2 can be solved. The other two equations represent the frictional reaction force and torque in terms of $f_1$and f_2:

$$f_{c1} = k_s(f_1 + f_2), \tag{125}$$

$$m_{c1} = k_r r(f_1 + f_2). \tag{126}$$

Since the both sides of (125) and (126) are functions of multipliers $\boldsymbol{\eta}$, these two equations serve as the complement equation for solving the multipliers $\boldsymbol{\eta}$.

7.3 Revolute joints

A revolute joint consists of a pair of bearing and a journal as illustrated in Fig. 9. Compared to a cylindrical joint, the revolute joint has two additional possible contact points located respectively at the centers of two end cross sections of the journal, to prevent the journal from relative sliding with respect to the bearing. The associated horizontal contact forces exerted on the journal can be expressed as

$$\mathbf{g}_{n3} = g_3\mathbf{e}_1; \qquad \mathbf{g}_{n4} = -g_4\mathbf{e}_1, \tag{127}$$

where g_3 and g_4 are magnitudes of the contact forces indicated in Fig. 9. Because of the axial clearance, the journal cannot contact the left and right wall of the bearing simultaneously. Therefore, contact forces g_3 and g_4 should satisfy the complementary condition:

$$0 \le g_3 \perp g_4 \ge 0. \tag{128}$$

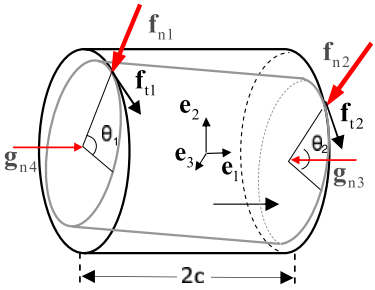

Fig. 9 Contacts in a revolute joint

Under the assumption that the journal is fixed on the inboard body of the joint, the relative velocities of the lateral contact points with respect to the bearings are given respectively as

$$\mathbf{v}_1 = -\omega_r\, \mathbf{e}_1 \times r(\cos\theta_1 \mathbf{e}_3 + \sin\theta_1 \mathbf{e}_2), \tag{129}$$

$$\mathbf{v}_2 = -\omega_r\, \mathbf{e}_1 \times r(\cos\theta_2 \mathbf{e}_3 + \sin\theta_2 \mathbf{e}_2), \tag{130}$$

where $\omega_r \mathbf{e}_1$ is the joint angular velocity, θ_1 and θ_2 are orientation angles of the contact points as shown in Fig. 9 and r is the radius of the journal. The associated normal contact forces exerted on the journal can be expressed as

$$\mathbf{f}_{n1} = -f_1 \cos\theta_1 \mathbf{e}_3 - f_1 \sin\theta_1 \mathbf{e}_2, \tag{131}$$

$$\mathbf{f}_{n2} = -f_2 \cos\theta_2 \mathbf{e}_3 - f_2 \sin\theta_2 \mathbf{e}_2. \tag{132}$$

Based on the Coulomb law of friction, the corresponding frictional contact forces exerted on the journal are given as

$$\mathbf{f}_{t1} = f_1 k_r(-\cos\theta_1 \mathbf{e}_2 + \sin\theta_1 \mathbf{e}_3), \tag{133}$$

$$\mathbf{f}_{t2} = f_2 k_r(-\cos\theta_2 \mathbf{e}_2 + \sin\theta_2 \mathbf{e}_3), \tag{134}$$

where the general coefficient of friction is

$$k_r = \mu\, \mathrm{sign}(\omega_r). \tag{135}$$

The reaction force $\mathbf{f}_c = f_{c1}\mathbf{e}_1 + f_{c2}\mathbf{e}_2 + f_{c3}\mathbf{e}_3$ and the torque $\mathbf{m}_c = m_{c1}\mathbf{e}_1 + m_{c2}\mathbf{e}_2 + m_{c3}\mathbf{e}_3$ at the center of the joint are equivalent to the contact forces system, which yields

$$\begin{pmatrix} f_{c2} \\ f_{c3} \\ m_{c2} \\ m_{c3} \end{pmatrix} = \begin{bmatrix} -k_r & -1 & -k_r & -1 \\ -1 & k_r & -1 & k_r \\ -c & k_r c & c & -k_r c \\ k_r c & c & -k_r c & -c \end{bmatrix} \begin{pmatrix} f_1 \cos\theta_1 \\ f_1 \sin\theta_1 \\ f_2 \cos\theta_2 \\ f_2 \sin\theta_2 \end{pmatrix}. \tag{136}$$

Substituting the solution of f_1 and f_2 into the following equation,

$$m_{c1} = \mu r(f_1 + f_2) \tag{137}$$

gives the complement equation for solving the multipliers $\boldsymbol{\eta}$.

If the horizontal contact forces are required for some purpose, they can be solved by the combination of the complementary condition (128) and the following equation:

$$f_{c1} = g_3 - g_4. \tag{138}$$

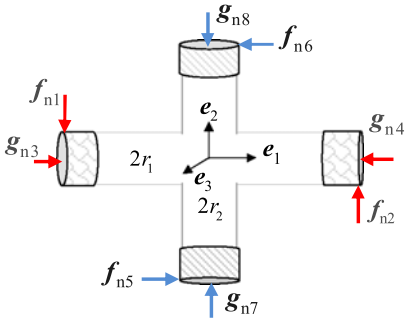

Fig. 10 Contacts in a universal joint

The solution is easily obtained:

$$g_3 = f_{c1}; \qquad g_4 = 0 \quad (\text{when } f_{c1} > 0), \tag{139}$$

$$g_4 = -f_{c1}; \qquad g_3 = 0 \quad (\text{when } f_{c1} < 0). \tag{140}$$

In practice, there are various types of revolute joints. Some of them are much more complicated in construction than the simplest one studied in this paper. The contact analysis about such joints is beyond the scope of this paper.

7.4 Universal joints

A universal joint can be taken as the combination of a horizontal revolute joint and a vertical revolute joint, as illustrated in Fig. 10 where r_1 and r_2 are the radius of the two journals. The horizontal joint is assumed to be fixed on the inboard body.

In terms of θ_1 and θ_2 the orientation angles of the contact points on the lateral surface of the horizontal journal, the normal contact forces $\mathbf{f}_{n1}$ and $\mathbf{f}_{n2}$ are expressed as

$$\mathbf{f}_{n1} = -f_1 \cos\theta_1 \mathbf{e}_3 - f_1 \sin\theta_1 \mathbf{e}_2, \tag{141}$$

$$\mathbf{f}_{n2} = -f_2 \cos\theta_2 \mathbf{e}_3 - f_2 \sin\theta_2 \mathbf{e}_2. \tag{142}$$

At the geometric center of the universal joint, the reaction force $\mathbf{f}_c = f_{c1}\mathbf{e}_1 + f_{c2}\mathbf{e}_2 + f_{c3}\mathbf{e}_3$ and the torque $\mathbf{m}_c = m_{c1}\mathbf{e}_1 + m_{c2}\mathbf{e}_2 + m_{c3}\mathbf{e}_3$ exerted on the horizontal journal, as a force system, is equivalent to the contact force system on the journal. Following the same procedure described in Sect. 7.3, one obtains

$$\begin{pmatrix} f_{c2} \\ f_{c3} \\ m_{c2} \\ m_{c3} \end{pmatrix} = \begin{bmatrix} -k_1 & -1 & -k_1 & -1 \\ -1 & k_1 & -1 & k_1 \\ -c_1 & k_1 c_1 & c_1 & -k_1 c_1 \\ k_1 c_1 & c_1 & -k_1 c_1 & -c_1 \end{bmatrix} \begin{pmatrix} f_1 \cos\theta_1 \\ f_1 \sin\theta_1 \\ f_2 \cos\theta_2 \\ f_2 \sin\theta_2 \end{pmatrix}, \tag{143}$$

where

$$k_1 = \mu \operatorname{sign}(\omega_{r1}) \tag{144}$$

and $\omega_{r1}\mathbf{e}_1$ is the angular velocity of the horizontal revolute joint. The normal contact forces on the lateral surface of the vertical journal can be written as

$$\mathbf{f}_{n5} = -f_5 \cos\theta_3 \mathbf{e}_1 - f_5 \sin\theta_3 \mathbf{e}_3, \tag{145}$$

$$\mathbf{f}_{n6} = -f_6 \cos\theta_4 \mathbf{e}_1 - f_6 \sin\theta_4 \mathbf{e}_3, \tag{146}$$

where θ_3 and θ_4 are the orientation angles of the corresponding contact points. Based on the common assumption that the cross shaft in a universal joint is massless, the contact force system exerted on the vertical journal and the contact force system exerted on the horizontal journal compose a balanced force system. Therefore, replacing $\mathbf{f}_c, \mathbf{m}_c\mathbf{e}_1, \mathbf{e}_2, \mathbf{e}_3$ in (122) and (123) with $-\mathbf{f}_c, -\mathbf{m}_c, \mathbf{e}_2, \mathbf{e}_3, \mathbf{e}_1$, respectively, one obtains

$$\begin{pmatrix} -f_{c3} \\ -f_{c1} \\ -m_{c3} \\ -m_{c1} \end{pmatrix} = \begin{bmatrix} -k_2 & -1 & -k_2 & -1 \\ -1 & k_2 & -1 & k_2 \\ -c_2 & k_2c_2 & c_2 & -k_2c_2 \\ k_2c_2 & c_2 & -k_2c_2 & -c_2 \end{bmatrix} \begin{pmatrix} f_5\cos\theta_3 \\ f_5\sin\theta_3 \\ f_6\cos\theta_4 \\ f_6\sin\theta_4 \end{pmatrix}, \tag{147}$$

where

$$k_2 = \mu\,\mathrm{sign}(\omega_{r2}) \tag{148}$$

and $\omega_{r2}\mathbf{e}_2$ is the angular velocity of the vertical revolute joint. The complement equations for solving the multipliers $\boldsymbol{\eta}$ are as follows:

$$m_{c1} = \mu r_1(f_1 + f_2), \tag{149}$$

$$-m_{c2} = \mu r_2(f_5 + f_6). \tag{150}$$

8 Numerical examples

In this section, three examples involving different types of joints with friction are given to demonstrate the application of the methodology presented in this paper.

8.1 Single pendulum with spherical joint

As is shown in Fig. 11, a single pendulum is connected to the ground with a spherical joint whose ball is 0.05 m in radius and fixed on the pendulum. The pendulum is a rectangular block with 1.0 m in length, 0.1 m in width and 0.1 m in height. It is made of steel with density 7800 kg/m^3. The friction in the spherical joint is taken into account and the coefficient of friction is assumed to be 0.6. Initially the pendulum is at rest in the horizontal position, and will swing afterward under the action of gravity.

The motion of the pendulum during the first 10 seconds is simulated respectively with ADAMS and the software based on the method proposed in this paper. Comparative results are shown in Fig. 12 and Fig. 13. The results of ADAMS and this paper are consistent in tendency but not exactly identical.

By careful observation, we found that the joint reaction force at the center of the ball is treated as the normal contact force by ADAMS, or more precisely, the equation

$$\mathbf{m}_c = \frac{\mu r \mathbf{f}_c \times (\boldsymbol{\omega}_r \times \mathbf{f}_c)}{\sqrt{\mathbf{f}_c \cdot \mathbf{f}_c}} \tag{151}$$

is used by ADAMS to calculate the frictional torque, not (110). Since the joint reaction force $\mathbf{f}_c$ is greater than the normal contact force in magnitude, as indicated by (111), the frictional torque approximated by (151) is larger than the actual value and causes more energy dissipation. This is the main reason for the inconsistence shown in Fig. 12 and Fig. 13.

In order to verify our observation, we redo the analysis according to (151). As indicated in Fig. 14 and Fig. 15, the results of this paper and ADAMS are exactly the same during

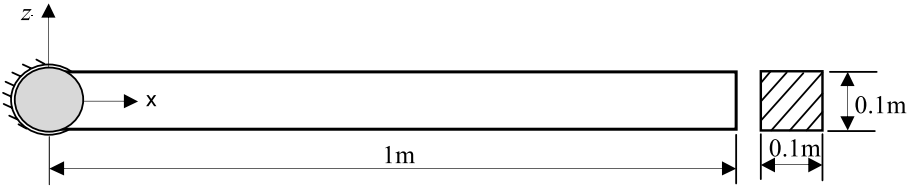

Fig. 11 Single pendulum with spherical joint

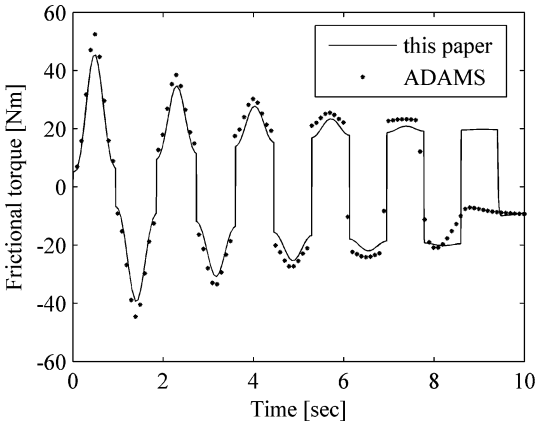

Fig. 12 Frictional torque in the spherical joint

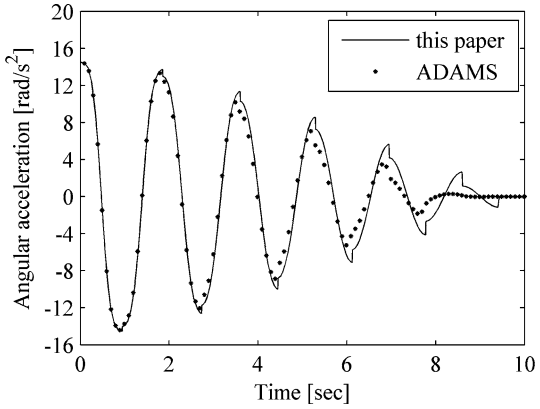

Fig. 13 Angular acceleration of the spherical joint

the period of the first 7.7 seconds in this case. This shows that ADAMS really uses (151) to approximate the frictional torque.

At the instant of 7.7 seconds, both of the angular velocity and the acceleration of the pendulum are close to zero, and the frictional torques given respectively by this paper and ADAMS begin to depart from each other, while the angular accelerations are still in good agreement. Such a deviation is caused by computational errors. As illustrated by Fig. 6, the velocity tolerance v_ε can change the numerical solution at the moment when the relative velocity is close to zero. In general, the smaller the v_ε is, the better the numerical solutions will be. However, if the velocity tolerance is too small, the speed of solution will be slowed down significantly. In this paper, v_ε is 10^{-4} m/s.

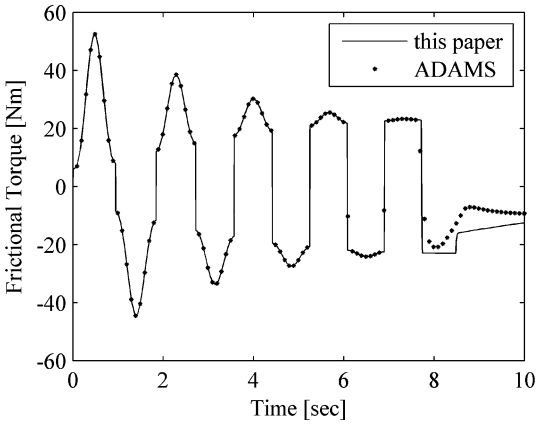

Fig. 14 Frictional torque according to (151)

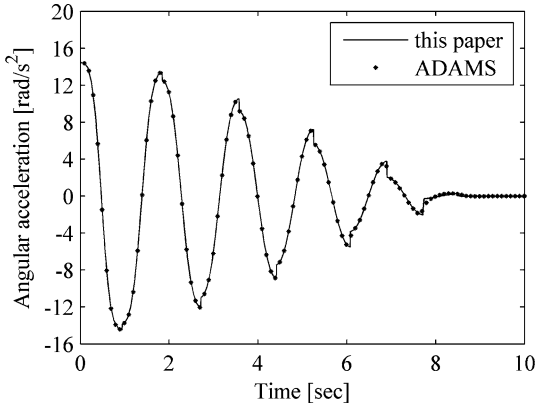

Fig. 15 Angular acceleration according to (151)

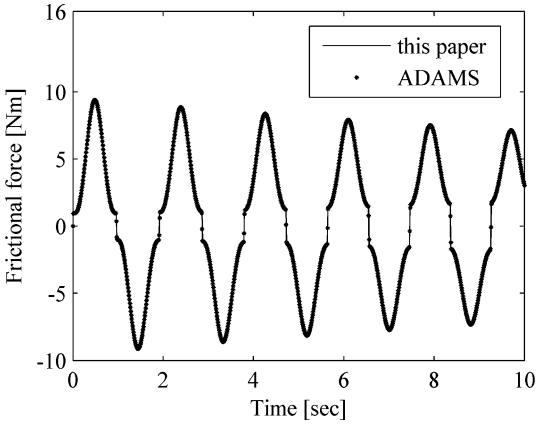

Fig. 16 Frictional torque with frictional coefficient $\mu = 0.1$

After the instant is close to 10 seconds, the pendulum is in the sticking state, which can be observed in Fig. 13. The numerical values of the angular velocities are not exactly zeros, but oscillate around zero with small amplitudes that depend on the velocity tolerance v_ε.

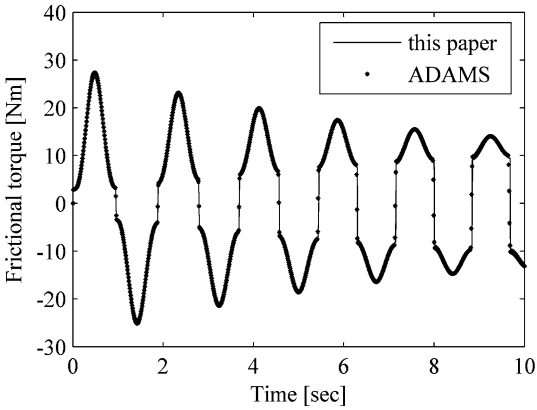

Fig. 17 Frictional torque with frictional coefficient $\mu = 0.3$

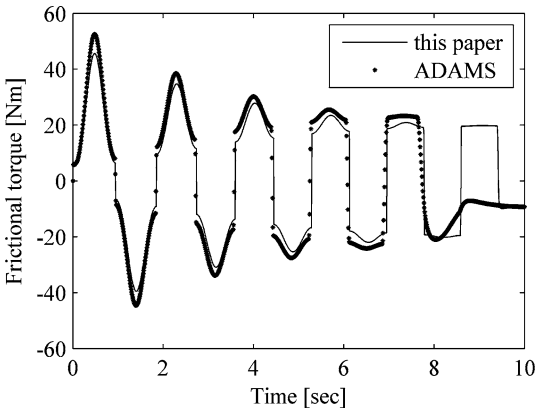

Fig. 18 Frictional torque with frictional coefficient $\mu = 0.6$

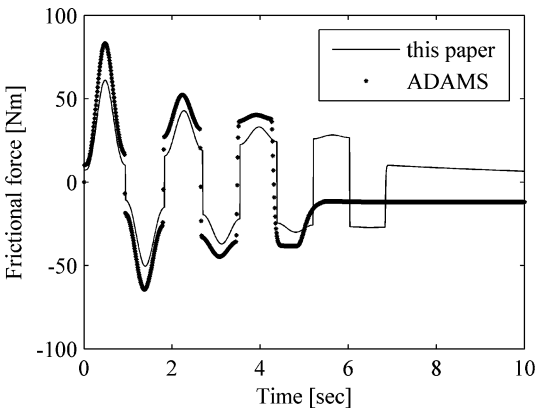

Fig. 19 Frictional torque with frictional coefficient $\mu = 1$

On the other hand, the differences between (151) and (110) may be slight or great depending on the coefficient of friction. It is shown by Fig. 16, Fig. 17, Fig. 18, and Fig. 19 that, with the increase of the frictional coefficient, the differences become greater.

One of the advantages of the method presented in this paper is the capability of obtaining the details about the contacts in a joint. For example, the history of the normal contact forces

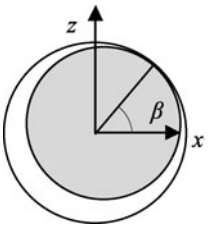

Fig. 20 Definition of contact angle

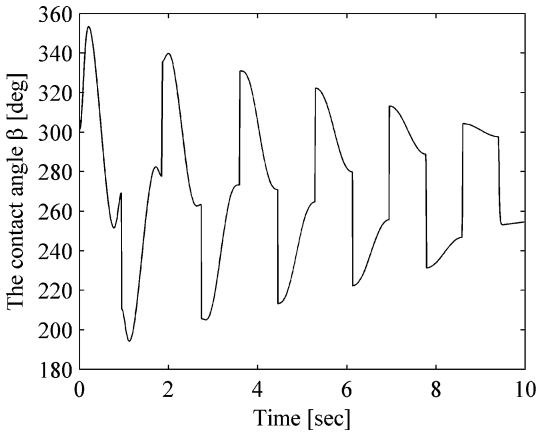

Fig. 21 Orientation of the contact point

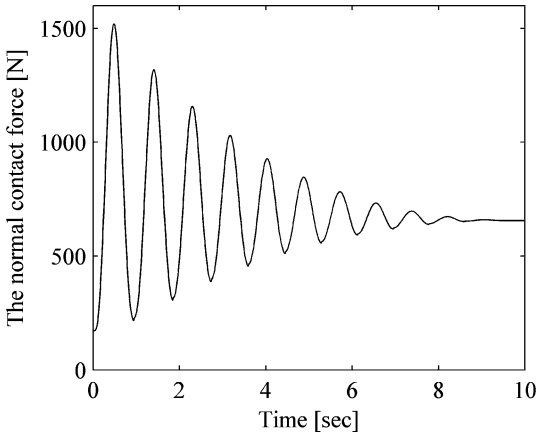

Fig. 22 Normal contact force on the ball

and the contact positions can be obtained during the simulation of this example. Since the contact point is always on the XZ plane as shown in Fig. 11, the contact angle β, illustrated in Fig. 20, is sufficient for the description of the contact orientation. Figure 21 and Fig. 22 describe the variation of the contact position and the normal contact force, respectively.

It can be observed that the normal contact force on the ball decreases continuously but does not vanish when the pendulum stops moving. That means the static frictional torque exists in the spherical joint, as shown in Fig. 22.

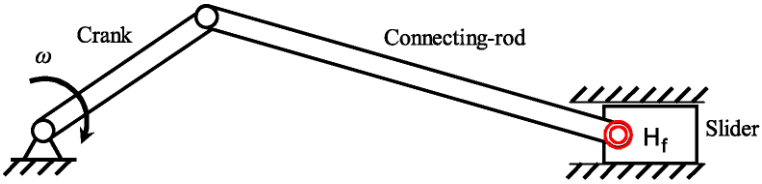

Fig. 23 A crank-slider mechanism

As is shown in Fig. 21, at some instants, the values of the contact angle change suddenly. Therefore, the impacts will occur at these moments, provided the previous impacts have not made noticeable differences in the dynamics of the system.

It is worth noting that we can learn many things about possible impacts by the method presented in this paper, in spite of the assumption of noncolliding contacts.

8.2 Crank-slider mechanism

The second example deals with a crank-slider mechanism as shown in Fig. 23. The crank is 0.5 m in length, 0.1 m in width, and 0.1 m in height. The connecting rod is 1 m in length, 0.1 m in width, and 0.1 m in height. The slider is a cube of 0.2 m on each edge. They are all made of steel with a density of 7801 kg/m^3. The coefficient of friction for the revolute joint H_f that links the connecting-rod and the slider is 0.3. Its journal is 0.01 m in radius and 0.1 m in length. Other joints in the mechanism are assumed to be ideal joints.

The applied forces consist of force of gravity and the driving moment that make the crank rotate at a constant angular velocity $\omega = 10$ rad/s. At the initial time, the whole system is in the horizontal position.

The velocity and the acceleration of the mass center of the slider are plotted in Fig. 24. Curves with solid line and marker o indicate the results given by this paper and ADAMS, respectively. As can be seen in Fig. 24, the numerical results obtained in this paper are almost the same with ADAMS.

The frictional torques of joint H_f obtained by this paper and ADAMS, respectively, are compared. As shown in Fig. 25, they are generally in agreement with each other. However, ADAMS computes the frictional torque using the equation

$$m_c^1 = \mu R \|\mathbf{f}_c\| \tag{152}$$

which is different from (137) used in this paper. It can be verified that, when the coefficient of friction is small, the differences between (137) and (152) will be greatly reduced under the conditions of the normal contact forces f_1 and f_2 are equivalent and the contact angles θ_1 and θ_2 are also equivalent. These conditions are satisfied in this example, as indicated in Fig. 26 and Fig. 27.

It can be seen in Fig. 26 and Fig. 28, there are sudden changes in the values of contact angles. However, some of them do not indicate impacts but result from the manner when an angle is represented by a real number. For example, an angle of 0° is actually the same with an angle of 360°. At some points of the curve, such as the point 3 in Fig. 28, the value of contact angle changes from 360° to 0° instantly, but these sudden changes do not have specific physical meanings. In order to better understand the dynamic behavior of the system, we plot the curve of the contact angle and the curve of angular velocity of the connecting-rod simultaneously on Fig. 28. To make the comparison more clear, the value

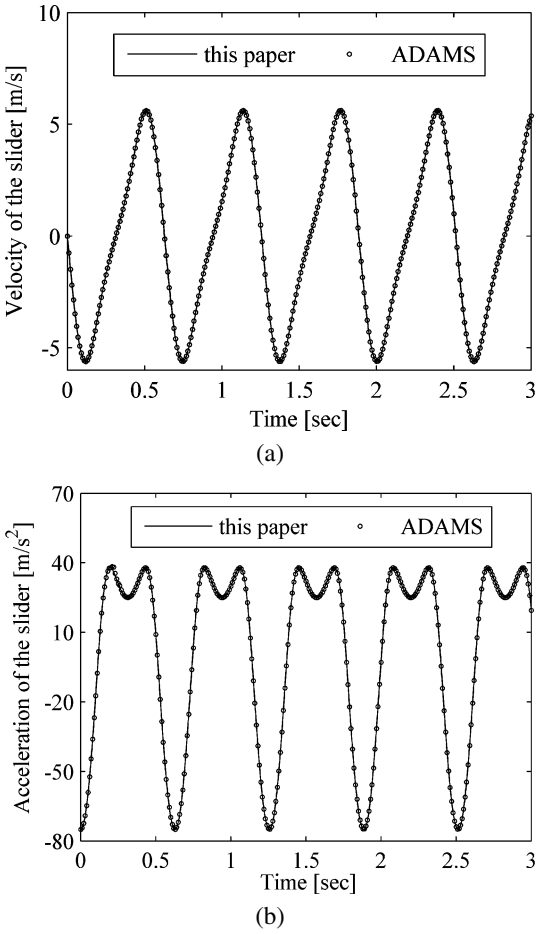

Fig. 24 (**a**) Velocity of mass center of the slider. (**b**) Acceleration of mass center of the slider

of the angular velocities is amplified by 10 times. It can be observed that, in a period of rotation, the contact angel changes abruptly at two instants, as shown at point 1 and point 2 in Fig. 28, when the angular velocity of the connecting-rod reverses its direction, as illustrated in Fig. 29.

8.3 Double pendulum

As shown in Fig. 30, the double pendulum system consists of two simple pendulums, whose material and shape are identical with the pendulum introduced in the first example. The first pendulum is connected to the ground by a frictional cylindrical joint. This cylindrical joint is fixed on the pendulum with the shaft of 0.05 m in radius and the guide of 0.3 m.

The first pendulum is armed by another pendulum with a frictional universal joint whose two shaft axles are both 0.01 m in radius and 0.1 m in length. The coefficient of friction is 0.3. At the initial time, the two pendulums are in the horizontal position and move along the guide at the velocity $v = 10$ m/s.

Firstly, the motion of the pivot of the cylindrical joint is studied. It is seen in Fig. 31, the pivot moves 13.76 m along the shaft and stops at the moment around 4.5 seconds. However, at this moment, the numerical value of the velocity of the pivot is not exactly zero

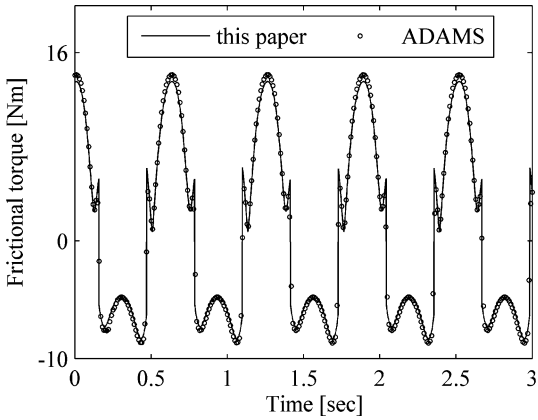

Fig. 25 Frictional torque of joint H_f

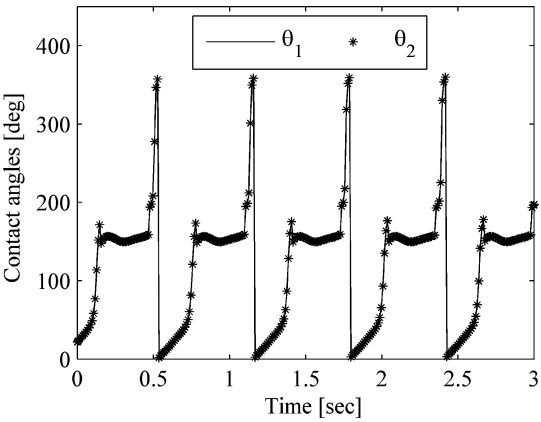

Fig. 26 Contact angles of the contact points in joint H_f

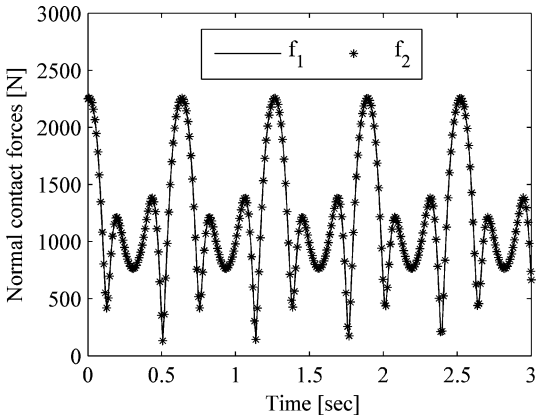

Fig. 27 Normal contact forces in joint H_f

because the Coulomb's law of friction is replaced by the approximated formulas illustrated in Fig. 6. But the velocity of the pivot never exceeds 0.01 m/s in magnitude after the instant of 4 seconds as indicated in Fig. 32.

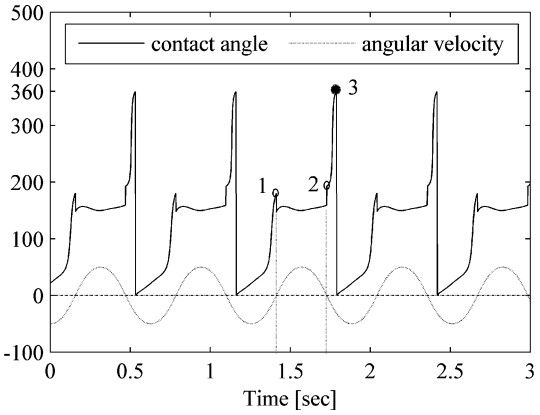

Fig. 28 Variation of contact angle in joint H_f with respective to the angular velocity of the connecting-rod

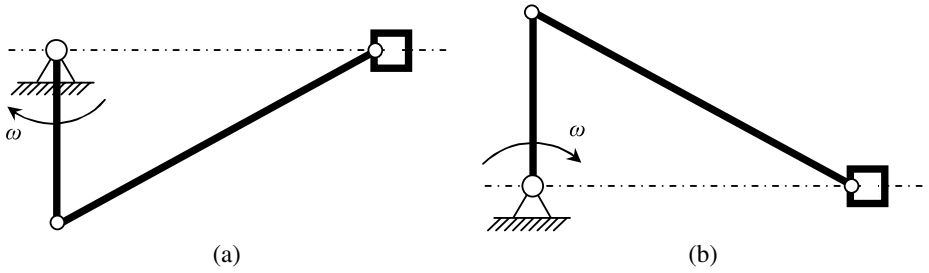

Fig. 29 Two configurations of the crank-slider mechanism associated with two possible impacts

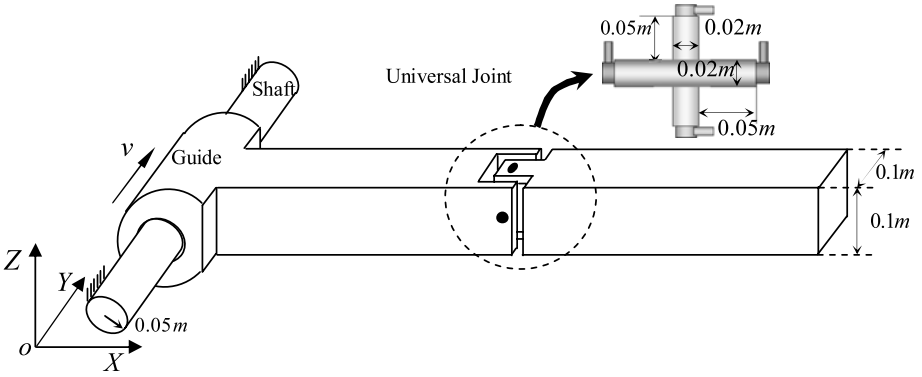

Fig. 30 Double pendulum

Figure 33 shows the numerical results of the angular velocity of the first pendulum. We can see that, after the pivot is at rest, the first pendulum is still in motion in a manner like a revolute joint and finally at rest in the vertical position as indicated in Fig. 34, where the swing angle is defined as the angle between the y axis and the direction along the length of the first pendulum. During this relative long time (60 seconds) simulation, the numerical solutions go smoothly. This verifies the method presented in this paper is numerically stable in this case.

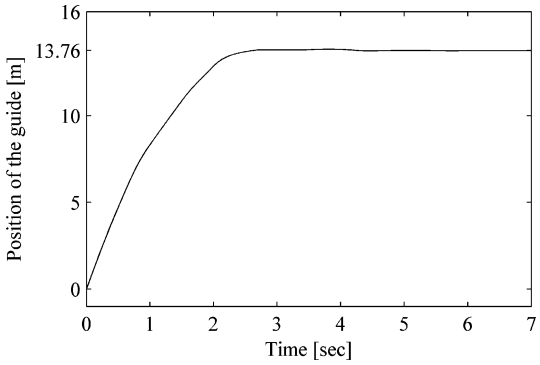

Fig. 31 Position of the guide of the cylindrical joint

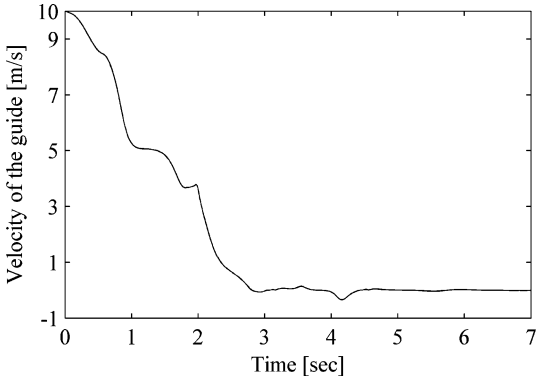

Fig. 32 Velocity of the guide of the cylindrical joint

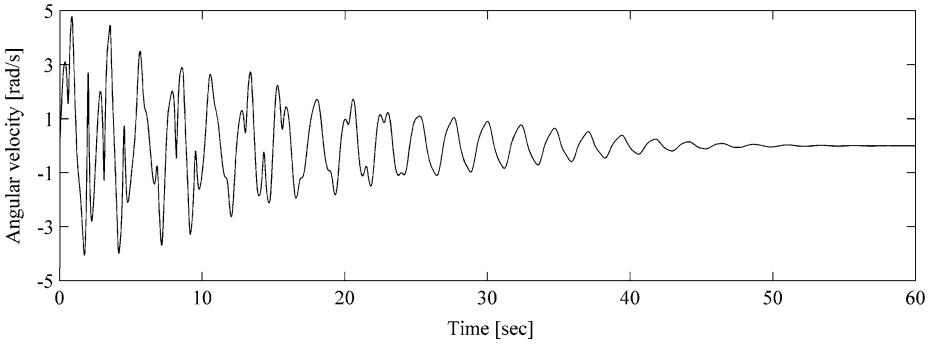

Fig. 33 Angular velocity of the first pendulum

Since the stiff problem involved in the contact detection is avoided, the method presented in this paper can be applied in the contact analysis of spatial frictional joints. Figure 35 and Fig. 36 are the frictional forces and torques in the two joints, respectively. It can be seen that, the frictional force in cylindrical joint lasts about 10 seconds after the pivot is at rest, which indicates the frictional force in this period is static. This results from the non-vanishing reaction forces of the universal joint. From Fig. 36, one can see that the friction torques around x and y axis vanish after about 17 seconds. From then on, the behavior of the whole system is much like the system with two pendulums linked by revolute joints.

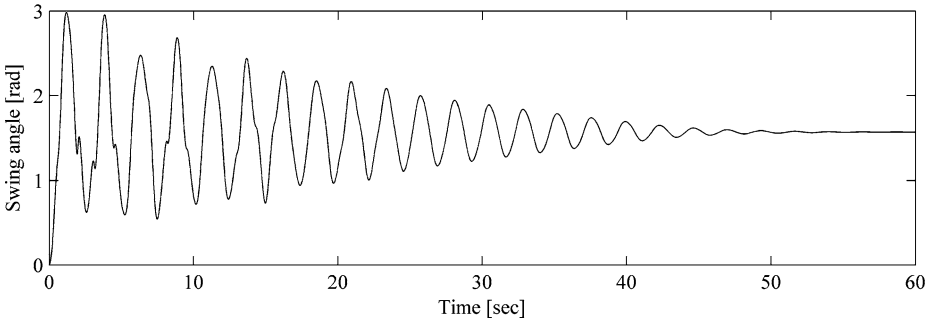

Fig. 34 Swing angle of the first pendulum

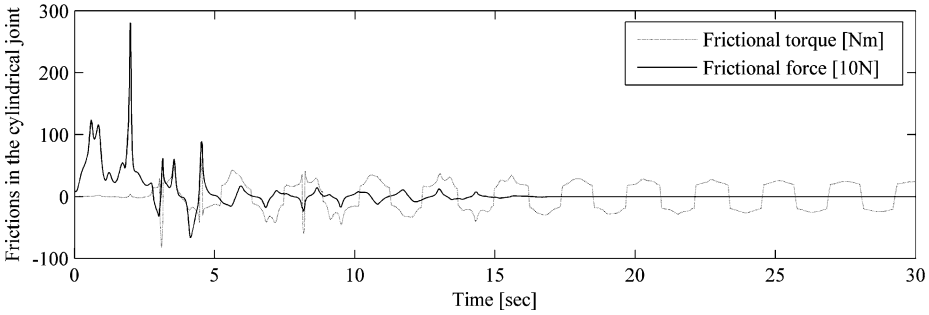

Fig. 35 Frictional forces and torques in the cylindrical joint

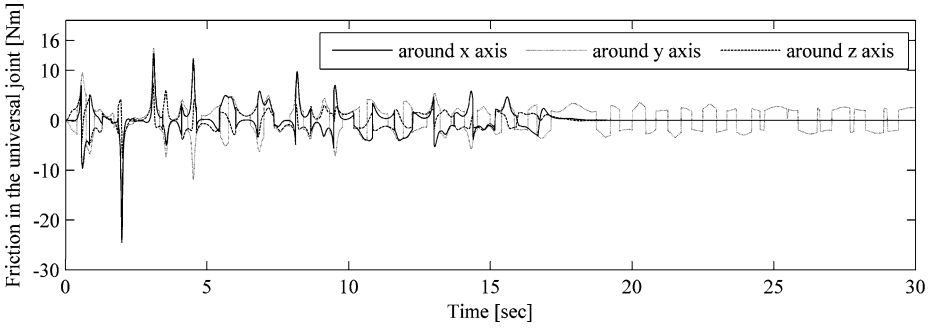

Fig. 36 Friction in the universal joint before 30 seconds

The orientation angles θ_1 and θ_2 of the two contact points in the cylindrical joint are obtained. As shown in Fig. 37, the movement along the guide makes θ_1 and θ_2 different from each other. Figure 38 gives the time history of the normal contact forces in the cylindrical joint, from which one can observe that they are initially different from each other and then gradually become consistent. Comparing it with Fig. 37, one can see that, the differences between contact angles have a significant effect on the normal contact forces.

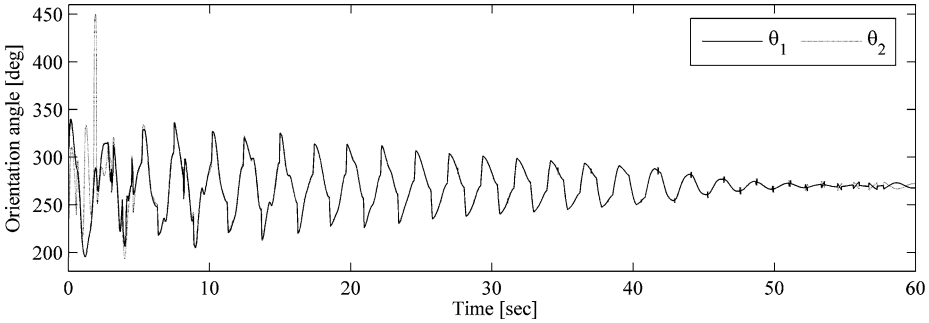

Fig. 37 Orientation angles of the two contact points in the cylindrical joint

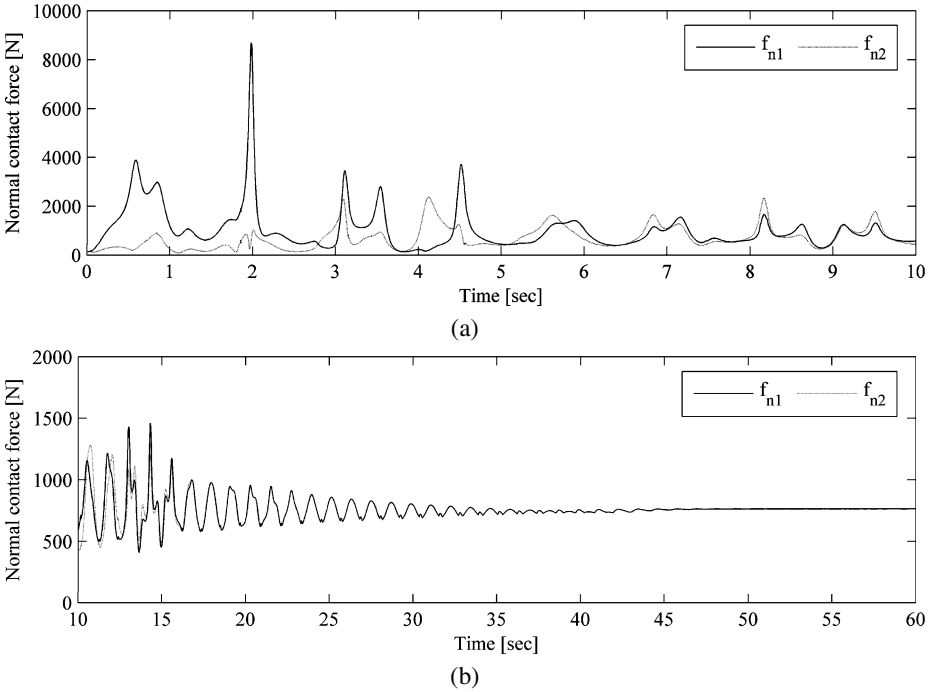

Fig. 38 (**a**) Time history of the normal contact forces in the cylindrical joint before the 10 seconds. (**b**) Time history of the normal contact forces in the cylindrical joint after the 10 seconds

9 Conclusions

Both joint reaction forces and contact forces in the joint can be taken as a force system. Moreover, the two force systems are equivalent, providing six equations related joint reaction forces with joint contact forces. Combining these equations and unilateral contact conditions, one can obtain the contact forces and locations. This important fact has not been fully realized in the existing methods for contact analysis.

As it is well known, the joint reaction forces of a cut joint, which is usually treated as part of the unknown applied forces, must be associated with the joint constraint equations to make the motion equations solvable. In the same principle, the unknown frictional forces

must be associated with some complement equations. The six equivalence relations between the joint reaction force system and the contact force system provide such complement equations. As is shown in this paper, the contact forces and locations at a joint can be described in terms of a few parameters. In connection with classic joints except prismatic joints, the number of these parameters is less than six. That is to say, these parameters can be solved by only part of the equivalence relations, and the remainders are just the required complement equations for frictional forces.

In the method presented in this paper, the joint reaction forces are calculated frequently. In order to improve the computational efficiency, a recursive formulation is presented based on the interactions between bodies in a multibody system. From a mathematic point of view, the proposed formulation is not new. However, the physical insight behind the traditional recursive formulation for open loop systems is explored in this paper. We also explained articulated inertias and employed them in a different manner. In the proposed formulation, both the inverse and the assembly of system mass matrices are avoided. More importantly, the joint reaction forces can be obtained easily with the proposed method. In comparison with some of the existing methods for noncolliding contact analysis, such as the method used by ADAMS, one of the advantages of presented method is that the details about contacts at a joint, such as the time history of the contact force, the contact position, etc. can be obtained during the simulation. In spite of the assumption of impact free, the instants of possible impacts can be detected without relying upon any ambiguous parameters, as indicated by the numerical examples in this paper.

Acknowledgement This research was supported by the China National Science Foundation under grant No. 10972044 and 2006CB705400.

References

1. Flores, P., Ambrósio, J., Claro Pimenta, J., Lankarani, H.: Kinematics and Dynamics of Multibody Systems with Imperfect Joints: Models and Case Studies. Springer, Dordrecht (2008)
2. Gilardi, G., Sharf, I.: Literature survey of contact dynamics modeling. Mech. Mach. Theory **37**(10), 1213–1239 (2002)
3. Glocker, C., Pfeiffer, F.: Dynamical systems with unilateral contacts. Nonlinear Dyn. **3**(4), 245–259 (1992)
4. Glocker, C., Pfeiffer, F.: Multiple impacts with friction in rigid multibody systems. Nonlinear Dyn. **7**(4), 471–497 (1995)
5. Glocker, C., Pfeiffer, F.: Complementarity problems in multibody systems with planar friction. Arch. Appl. Mech. **63**(7), 452–463 (1993)
6. Glocker, C., Studer, C.: Formulation and preparation for numerical evaluation of linear complementarity systems in dynamics. Multibody Syst. Dyn. **13**(4), 447–463 (2005)
7. Leine, R.I., van Campen, D.H., Glocker, C.: Nonlinear dynamics and modeling of various wooden toys with impact and friction. J. Vib. Control **9**(1–2), 25–78 (2003)
8. Glocker, C.: Concepts for modeling impacts without friction. Acta Mech. **168**(1–2), 1–19 (2004)
9. Djerassi, S.: Collision with friction; Part A: Newton's hypothesis. Multibody Syst. Dyn. **21**(1), 37–54 (2009)
10. Djerassi, S.: Collision with friction; Part B: Poisson's and Stornge's hypotheses. Multibody Syst. Dyn. **21**(1), 55–70 (2009)
11. Najafabadi, S.A.M., Kövecses, J., Angeles, J.: Impacts in multibody systems: modeling and experiments. Multibody Syst. Dyn. **20**(2), 163–176 (2008)
12. Schiehlen, W., Seifried, R.: Three approaches for elastodynamic contact in multibody systems. Multibody Syst. Dyn. **12**(1), 1–16 (2004)
13. Pang, J., Trinkle, J.C.: Complementarity formulations and existence of solutions of dynamic multi-rigid-body contact problems with Coulomb friction. Math. Program. **73**(2), 199–226 (1996)
14. Trinkle, J.C., Tzitzoutis, J., Pang, J.S.: Dynamic multi-rigid-body systems with concurrent distributed contacts: theory and examples. Philos. Trans. Math. Phys. Eng. Sci. Ser. A **359**(1789), 2575–2593 (2001)

15. Pfeiffer, F., Foerg, M., Ulbrich, H.: Numerical aspects of non-smooth multibody dynamics. Comput. Methods Appl. Mech. Eng. **195**(50–51), 6891–6908 (2006)
16. Förg, M., Pfeiffer, F., Ulbrich, H.: Simulation of unilateral constrained systems with many bodies. Multibody Syst. Dyn. **14**(2), 137–154 (2005)
17. Flores, P., Ambrósio, J., Claro, J.C.P., Lankarani, H.M., Koshy, C.S.: A study on dynamics of mechanical systems including joints with clearance and lubrication. Mech. Mach. Theory **41**(3), 247–261 (2006)
18. Flores, P., Ambrósio, J., Claro, J.C.P., Lankarani, H.M.: Influence of the contact-impact force model on the dynamic response of multibody systems. Proc. Inst. Mech. Eng., Part-K J. Multi-body Dyn. **220**(1), 21–34 (2006)
19. Gonthier, Y., McPhee, J., Lange, C., Piedboeuf, J.C.: A regularized contact model with asymmetric damping and dwell-time dependent friction. Multibody Syst. Dyn. **11**(3), 209–233 (2004)
20. Bing, S., Ye, J.: Dynamic analysis of the reheat-stop-valve mechanism with revolute clearance joint in consideration of thermal effect. Mech. Mach. Theory **43**(12), 1625–1638 (2008)
21. Srivastava, N., Haque, I.: Clearance and friction-induced dynamics of chain CVT drives. Multibody Syst. Dyn. **19**(3), 255–280 (2008)
22. Orden, J.C.G.: Analysis of joint clearances in multibody systems. Multibody Syst. Dyn. **13**(4), 401–420 (2005)
23. Liu, C.S., Zhang, K., Yang, L.: Normal force-displacement relationship of spherical joints with clearances. J. Comput. Nonlinear Dyn. **1**(2), 160–167 (2006)
24. Flores, P., Ambrósio, J., Claro, J.C.P., Lankarani, H.M.: Translational joints with clearance in rigid multibody systems. J. Comput. Nonlinear Dyn. **3**(1), 0110071-10 (2008)
25. Flores, P., Ambrósio, J., Claro, J.C.P., Lankarani, H.M.: Dynamics of multibody systems with spherical clearance joints. J. Comput. Nonlinear Dyn. **1**(3), 240–247 (2006)
26. Flores, P., Ambrósio, J.: Revolute joints with clearance in multibody systems. Comput. Struct. **82**(17–19), 1359–1369 (2004)
27. Flores, P., Ambrósio, J., Claro, J.C.P., Lankarani, H.M.: Spatial revolute joints with clearance for dynamic analysis of multibody systems. Proc. Inst. Mech. Eng., Part-K J. Multi-body Dyn. **220**(4), 257–271 (2006)
28. Inna, S., Yuning, Z.: A contact force solution for non-colliding contact dynamics simulation. Multibody Syst. Dyn. **16**(3), 263–290 (2006)
29. Paul, B.: Kinematics and Dynamics of Planar Machinery. Prentice-Hall, Englewood Cliffs (1979)
30. Hall, A.S.: Notes on Mechanism Analysis. Waveland Press Inc., Long Grove (1986)
31. Haug, E.J., Wu, S.C., Yang, S.M.: Dynamics of mechanical systems with Coulomb friction stiction, impact and constraint addition-deletion—I and II. Mech. Mach. Theory **21**(5), 401–425 (1986)
32. Bae, D.S., Haug, E.J.: A recursive formulation for constrained mechanical system dynamics. I. Open loop systems. Mech. Struct. Mach. **15**(3), 359–382 (1987)
33. Bae, D.S, Haug, E.J.: A recursive formulation for constrained mechanical system dynamics: Part II. Closed loop systems. Mech. Des. Struct. Mach. **15**(4), 481–506 (1987)
34. Kim, S.S., Haug, E.J.: A recursive formulation for flexible multibody dynamics. I. Open loop systems. Comput. Methods Appl. Mech. Eng. **71**(3), 293–314 (1988)
35. Kim, S.S., Haug, E.J.: A recursive formulation for flexible multibody dynamics. II. Closed-loop systems. Comput. Methods Appl. Mech. Eng. **74**(3), 251–269 (1989)
36. Hwang, Y.L.: Dynamic recursive decoupling method for closed-loop flexible mechanical systems. Int. J. Non-Linear Mech. **41**(10), 1181–1190 (2006)
37. Featherstone, R.: The calculation of robot dynamics using articulated-body inertias. Int. J. Robot. Res. **2**(1), 13–30 (1983)
38. Wittenburg, J.: Dynamics of Multibody Systems: Dynamics of Systems of Rigid Bodies. Springer, Berlin (2007)
39. Featherstone, R.: Robot Dynamics Algorithms. Kluwer Academic, Dordrecht (1987)
40. Leine, R.I., Glocker, Ch.: A set-valued force law for spatial Coulomb–Contensou friction. Eur. J. Mech.-A/Solids **22**(2), 193–216 (2003)
41. Leine, R.I., van de Wouw, N.: Stability properties of equilibrium sets of non-linear mechanical systems with dry friction and impact. Nonlinear Dyn. **51**(4), 551–583 (2008)
42. Pennestri, E., Valentini, P.P., Vita, L.: Multibody dynamics simulation of planar linkages with Dahl friction. Multibody Syst. Dyn. **17**(4), 321–347 (2007)
43. Rooney, G.T., Deravi, P.: Coulomb friction in mechanism sliding joints. Mech. Mach. Theory **17**(3), 207–211 (1982)